FLUID MECHANICAL INVESTIGATIONS OF CILIARY PROPULSION

Thesis by

Stuart Ronald Keller

In Partial Fulfillment of the Requirements

for the Degree of

Doctor of Philosophy

California Institute of Technology

Pasadena, California

1975

(Submitted May 27, 1975)

ACKNOWLEDGMENTS

It is with heart-felt emotion that I express my sincere gratitude to Professor Theodore Y. T. Wu. His personal warmth and estimable knowledge have been an inspiration to my personal and professional development.

Thanks are also due to Professor Milton Plesset and Dr. Christopher Brennen for some interesting discussions and thoughtful suggestions. I would also like to thank Dr. Howard Winet and Dr. Anthony T. W. Cheung for many stimulating conversations and for their invaluable advice and assistance on the biological portions of this work.

For their skillful aid and helpful recommendations on the preparation of this manuscript, I would like to express my sincere appreciation to Helen Burrus and Cecilia Lin.

Appreciation is also due to the Institute's Graduate Research Assistantship and Fellowship programs for financial assistance. Also I would like to express my gratitude to the National Science Foundation and the Office of Naval Research for financial support for part of this work.

ABSTRACT

Fluid mechanical investigations of ciliary propulsion are carried out from two points of view. In Part I, using a planar geometry, a model is developed for the fluid flow created by an array of metachronally coordinated cilia. The central concept of this model is to replace the discrete forces of the cilia ensemble by an equivalent continuum distribution of an unsteady body force within the cilia layer. This approach facilitates the calculation for the case of finite amplitude movement of cilia and takes into account the oscillatory component of the flow. Expressions for the flow velocity, pressure, and the energy expended by a cilium are obtained for small oscillatory Reynolds numbers. Calculations are carried out with the data obtained for the two ciliates Opalina ranarum and Paramecium multimicronucleatum. The results are compared with those of previous theoretical models and some experimental observations.

In Part II a model is developed for representing the mechanism of propulsion of a finite ciliated micro-organism having a prolate spheroidal shape. The basic concept of the model is to replace the micro-organism by a prolate spheroidal control surface at which certain boundary conditions on the fluid velocity are prescribed. These boundary conditions, which admit specific tangential and normal components of the flow velocity relative to the control surface, are proposed as a reasonable representation of the overall features of the flow field generated by the motion of the cilia system. Expressions are obtained for the velocity of propulsion, the rate of energy

dissipation in the fluid exterior to the cilia layer, and the stream function of the motion. The effect of the shape of the organism upon its locomotion is explored. Experimental streak photographs of the flow around both freely swimming and inert sedimenting Paramecia are presented and compared with the theoretical prediction of the streamlines.

TABLE OF CONTENTS

PART I

A TRACTION-LAYER MODEL FOR CILIARY PROPULSION

1. Introduction

Cilia are found in practically all the phyla of nature. Many micro-organisms are covered with cilia, the movement of which results in their vital locomotion. The palate of the frog is lined with cilia where their function is to maintain a constant cleansing flow of fluid. In man cilia are involved in the flow of mucous in the upper respiratory tract, the transport of gametes in the oviduct, and the circulation of the cerebrospinal fluid in which the brain is bathed.

A typical cilium is about 10 microns in length and has a circular cross section having a diameter of 0.2 microns. Although this investigation will not be concerned with the biophysics of how cilia move, it is worth noting that the internal structure of cilia has been found to be the same in many different organisms (Satir, 1974). In most ciliated systems, each cilium executes a periodic beat pattern which is indicated in Figure 1a. The numbers indicate successive positions of the cilium with a constant time interval between positions. The portion of the ciliary beat cycle during which the cilium is nearly straight and moving rapidly (positions 1-4) is referred to as the effective stroke, while the remainder of the cycle is termed the return stroke. While early observers (e.g. Gray, 1928) thought that all cilia execute planar beat patterns, it has recently been demonstrated that in various cases the cilia perform a three-dimensional beating motion (Cheung, 1973). For these cases it is often difficult to differentiate between an effective and a return stroke.

Cilia are normally distributed over the surface of cells in regular arrays. Although each cilium of an organism usually beats at

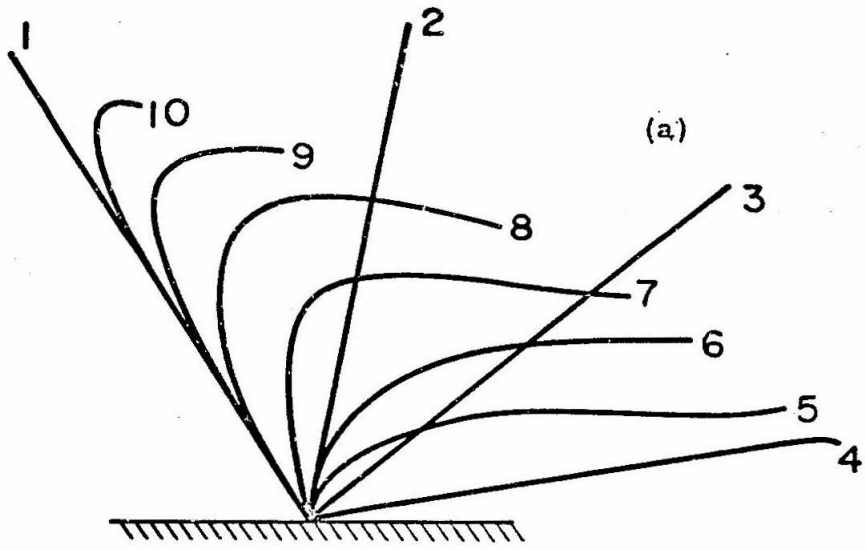

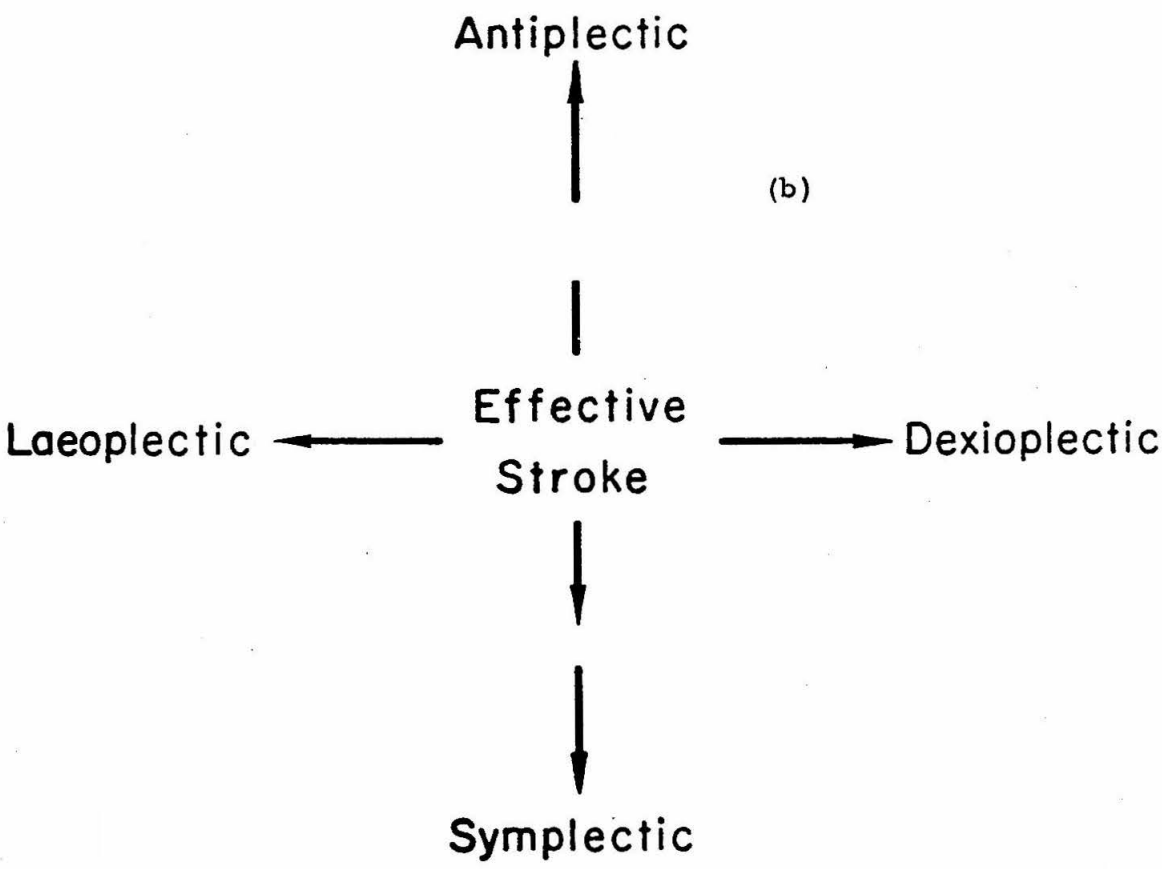

Fig. 1 a - Typical beat pattern of a cilium. b - The four basic types of metachrony.

the same rate, the cilia do not all beat in the same phase. The movements of adjacent cilia along the same row are exactly in phase, and these rows are each said to display synchrony. Neighboring cilia along any other direction are slightly out-of-phase and show metachrony. The cilia in files at right angles to the lines of synchrony show a maximum phase difference between neighbors, and waves of activity, metachronal waves, pass along the surface in these directions. The relationship between the direction of propagation of the metachronal waves and the direction of the effective stroke of the ciliary beat varies in different ciliated systems. The four basic types of metachrony were recognized and named by Knight-Jones (1954) as shown in Figure 1b. For symplectic metachrony the wave propagates in the same direction as the effective stroke, while for antiplectic metachrony the wave moves in the opposite direction. Laeoplectic and dextoplectic metachrony correspond to the situation where the wave moves in a direction perpendicular to that of the effective stroke. This nomenclature is inadequate, of course, for cilia not displaying a clearly defined effective stroke.

The movement of fluid by cilia poses an interesting fluid mechanical problem which has received considerable attention in the last quarter century. Two fundamental approaches to the problem have been advanced. The envelope model has been developed by several authors including Taylor (1951), Lighthill (1952), Blake (1971a, b, c), and Brennen (1974); it employs the concept of representing the ciliary propulsion by a waving material sheet enveloping the tips of the cilia. At the heart of the envelope approach is the pioneering work of Taylor

(1951) who considered the propulsion of an infinite waving sheet in a viscous, incompressible fluid, neglecting inertia forces. He found that the sheet would be propelled in a direction opposite to the direction of propagation of the wave with a speed $\frac{1}{2}(kh)^2 c$, where $k = 2\pi/\lambda$, λ being the wavelength, h is the wave amplitude, and c is the wave-speed. Taylor's analysis required that kh be much less than unity. The principal limitations of the envelope approach, as discussed in the review by Blake and Sleigh (1974), are due to the impermeability and no-slip conditions imposed on the flow at the envelope sheet (an assumption not fully supported by physical observations) and the mathematical necessity of a small amplitude analysis (for metachronal waves, kh is usually of order unity). Furthermore the envelope model is unsuitable for evaluating many important aspects of the problem that arise from the flow within the cilia layer.

In a different approach, Blake (1972) introduced the sublayer model for evaluating the flow within as well as outside the cilia layer by regarding each cilium as an individual slender body attached to an infinite flat plate in a regular array. The flow equations and the no-slip condition at the plate are satisfied by a distribution of Stokes flow force singularities along each cilium. The strength of these singularities is determined by considering the relative velocity between an individual cilium element and an "interaction velocity" which is taken to be the parallel steady flow which the rest of the ciliary array is supposed to create. The resulting complicated integral equations are then solved numerically for the mean velocity profile. As pointed out by Wu (1973) and Brennen (1974), the primary deficiency in the sublayer

model is caused by neglecting the oscillatory component of the "interaction velocity". From a physical standpoint, since the velocity of the cilia is typically 2 to 3 times the velocity of the mean flow they produce (Sleigh and Aiello, 1972), one might expect the magnitude of the oscillatory velocities to be considerable. Therefore the velocity that each cilium "sees" at any instant during its beat cycle is likely to be quite different from the parallel mean flow alone.

While the two existing theoretical approaches to ciliary propulsion have made important contributions to our understanding of a difficult problem, they also have some drawbacks. The purpose of this investigation is to present a new model for ciliary propulsion intended to rectify the deficiencies in the existing theoretical models. The main features of the model developed in this study are that it allows for finite amplitude movement of cilia and takes into account the oscillatory nature of the flow.

In Section 2 the geometry of the problem is described and the primary ideas are set forth. The central concept of the model is to replace the discrete forces generated by the cilia ensemble by an equivalent continuum distribution of an unsteady body force, the traction-layer. Expanding upon the prototype model of Wu (1973), we obtain in Section 3 a solution to the fundamental fluid mechanical equations satisfying the appropriate boundary conditions in terms of the unsteady body force field. In Section 4, using resistive theory, we derive an expression for the force exerted on the fluid by a segment of a cilium as a function of the motion of the cilium and the instantaneous flow field in which it is immersed. Using this expression in Section 5,

we outline a numerical procedure by which the body force field is determined from an analytical representation of the movement of a cilium and the instantaneous velocity of the local fluid. Further a simple and direct numerical iteration scheme is described by which the final velocity field is obtained. In Section 6 the results of the analysis are applied to the data obtained for the two ciliates Opalina ranarum and Paramecium multimicronuleatum. Finally in Section 7 we consider the energy expended by an individual cilium over one beat cycle.

2. Description of the model

In typical ciliated organisms the thickness of the cilia layer is small compared with the body dimensions. If L is the length of the cilium and $\mathcal{L}$ is a relevant body length, then it is observed that $L/\mathcal{L} < 0.1$ for most ciliated systems (see Tables 1 and 2). Consequently, as a first approximation, the geometry of the model may be taken as a hypothetical planar organism of infinite extent. The cilia are supposed to be distributed in a regular array of spacing a in the X direction and b in the Z direction in a Cartesian coordinate system fixed in the organism (see Figure 2). Each cilium is assumed to perform the same periodic beat pattern in an XY plane, with a constant phase difference between adjacent rows of cilia, such that the metachronal wave propagates in the positive X direction. This geometry allows both symplectic and antiplectic metachrony, with the extension to other types of metachrony being evident from the discussion.

For any ciliated organism, the basic agency of the motion is the combined effect of the forces exerted by each cilium on the fluid. In view of the difficulty in solving the fluid mechanical problem with a moving boundary so complicated as an ensemble of discrete cilia, an alternative formulation of the problem is developed. As already explained, the central concept of this model is to replace the discrete forces of the cilia ensemble by an equivalent continuum distribution of an unsteady body force field $\underline{F}(X, Y, t)$. The vector function $\underline{F}(X, Y, t)$ specifies the instantaneous force acting on a unit element of fluid centered at position (X, Y, Z) and at time t, the fluid element being of unit depth in the Z direction.

TABLE 1

EXPERIMENTALLY OBSERVED DATA FROM THE LITERATURE FOR OPALINA RANARUM

Quantity	Dimension	Symbol	Values		
Body length	μm	$\mathcal{L}$	150-500 [1]	200-300 [3]	220-360 [2]
Body width	μm	$\mathcal{W}$	100-300 [1]	130-230 [3]	160-250 [2]
Body thickness	μm	$\mathcal{T}$	20 [1]	20 [2]	20 [3]
Cilium length	μm	L	10-20 [4]	18 [5]	10-14 [8]
Cilium radius	μm	r_o	0.1 [6]		
Metachrony			symplectic [5]	symplectic [8]	
Wave speed	μm/sec	c	100-200 [1]	250 [5]	
Beat frequency	1/sec	f	1-4 [4]	1.7-2.9 [1]	25-30 [8]
Speed of propulsion	μm/sec	U^{∞}			
Wavelength	μm	λ	5-30 [6]		
Row spacing	μm	a	1.6 [6]		
Cilia spacing	μm	b	0.4 [6]		

Sources: 1-Okajima (1953), 2-Ueda (1956), 3-Naitoh (1958), 4-Sleigh (1962), 5-Sleigh (1968), 6-Tamm and Horridge (1970), 7-Cheung (1973), 8-Cheung and Jahn (1975).

TABLE 2

EXPERIMENTALLY OBSERVED DATA FROM THE LITERATURE
FOR PARAMECIUM MULTIMICRONUCLEATUM

Quantity	Dimension	Symbol	Values			
Body length	μm	$\mathscr{L}$	251 [8]	227 [9]	168-280 [1]	150-250 [7]
Body width	μm	$\mathscr{W}$	91 [9]	42-77 [1]		
Body thickness	μm	$\mathscr{T}$				
Cilium length	μm	L	12 [5]	10-12 [2]	10 [7]	
Cilium radius	μm	r_o	0.14 [2]			
Metachrony			antiplectic [4]	dexioplectic [8]		
Wave speed	μm/sec	c	340 [8]	712 [4]		
Beat frequency	1/sec	f	28 [5]	32 [8]		
Speed of propulsion	μm/sec	U^{∞}	156-545 [9]	2173-4166 [1]		
Wavelength	μm	λ	10-14 [8]			
Row spacing	μm	a	1.5 [6]			
Cilia spacing	μm	b	2.5 [6]			

Sources: 1-Bullington (1930), 2-Sedar and Porter (1955), 3-Sleigh (1960), 4-Sleigh (1962), 5-Parducz (1967), 6-Sleigh (1969), 7-Machemer (1972a), 8-Machemer (1972b), 9-Winet (1973).

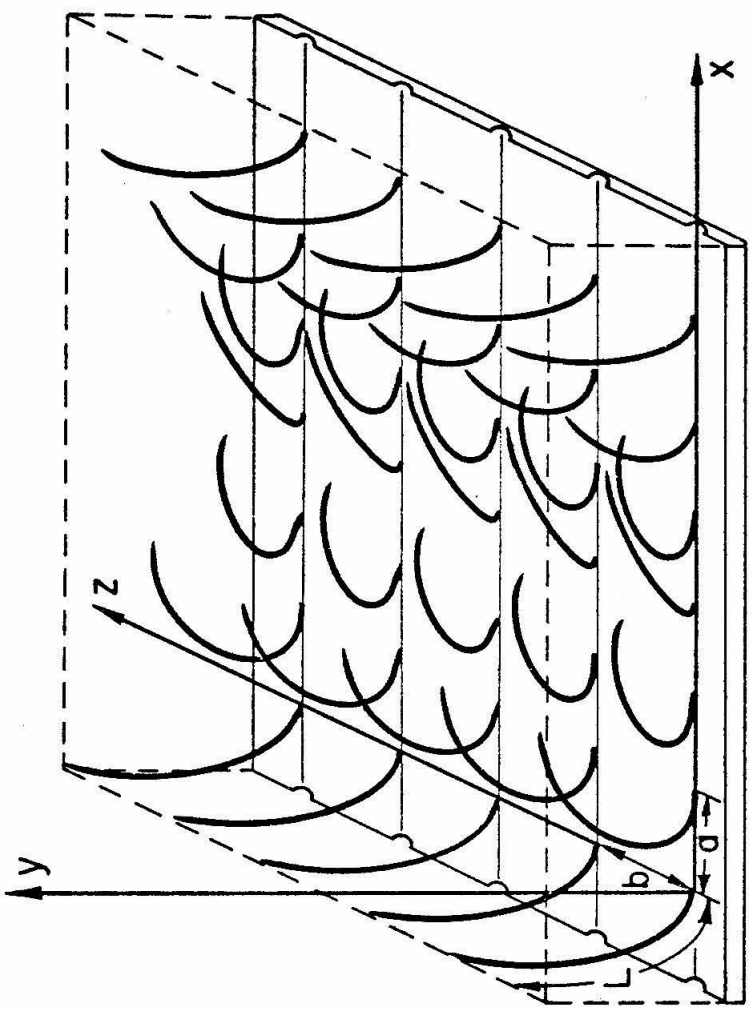

Fig. 2 Illustration of the coordinate system and regular array of cilia. The spacing in the X direction is a, while in the Z direction it is **b**.

For metachronal waves, $\underline{F}$ is a periodic function of $\phi(X,t) = kX-\omega t$, where ω is the angular frequency of the ciliary beat and $k = 2\pi/\lambda$, λ being the metachronal wavelength. Therefore $\underline{F}$ can be expanded in a Fourier series of the form

$$\underline{F}(X, Y, t) = \underline{F}_o(Y) + \sum_{n=1}^{\infty} \mathrm{Re}\,[\underline{F}_n(Y)\, e^{ni\phi}], \qquad (2.1)$$

where Re stands for the real part, $i = \sqrt{-1}$, and the Fourier coefficients $\underline{F}_n (n \geq 1)$ may be complex functions of Y. Further, since the cilia are of finite length L, $\underline{F}$ will vanish above the cilia layer, or equivalently

$$F(X, Y, t) = 0 \qquad \text{for} \quad Y > Y_L(kX-\omega t) \qquad (2.2)$$

where $Y = Y_L(kX-\omega t)$ is the thickness of the cilia layer, which depends on $\phi(X,t)$. The Fourier coefficients $\underline{F}_n$ corresponding to the distribution (2.1) will therefore vanish for $Y > L$, or

$$\underline{F}_n(Y) = 0 \quad \text{for} \quad Y > L, \quad n \geq 0. \qquad (2.3)$$

3. Solution of the fluid mechanical problem

The Navier-Stokes equations for the flow of an incompressible Newtonian fluid in two dimensions may be written as

$$P_{,X} = F + \rho\nu\nabla^2 U - \rho(U_{,t} + UU_{,X} + VU_{,Y}) \tag{3.1}$$

$$P_{,Y} = G + \rho\nu\nabla^2 V - \rho(V_{,t} + UV_{,X} + VV_{,Y}) \tag{3.2}$$

where P is the pressure, U and V are the X and Y components of velocity respectively, F and G are the X and Y components of body force $\underline{F}$, ρ is the density, and ν the kinematic viscosity. Here and in the sequel, "$_{,X}$", "$_{,Y}$", and "$_{,t}$" in subscript denote differentiation. The continuity equation, $U_{,X} + V_{,Y} = 0$, will be satisfied by a stream function Ψ defined by $U = \Psi_{,Y}$ and $V = -\Psi_{,X}$. If we non-dimensionalize all variables using k^{-1}, ω^{-1}, and $\rho\nu k^{-1}\omega^{-1}$ as the reference length, time and mass scales respectively, the equations of motion in non-dimensional variables (lower case) become

$$p_{,x} = f + \nabla^2\psi_{,y} - R_o(\psi_{,y\tau} + \psi_{,y}\psi_{,xy} - \psi_{,x}\psi_{,yy}) \tag{3.3}$$

$$p_{,y} = g - \nabla^2\psi_{,x} - R_o(\psi_{,x\tau} + \psi_{,y}\psi_{,xx} - \psi_{,x}\psi_{,xy}) \tag{3.4}$$

where $\tau = \omega t$, and $R_o = \omega/\nu k^2$ is the oscillatory Reynolds number which is taken to be much less than unity as is generally the case (Brennen, 1974). The x and y components of equation (2.1), after non-dimensionalization, become

$$f(x, y, \tau) = f_o(y) + \sum_{n=1}^{\infty} \mathrm{Re}\,[f_n(y)e^{ni(x-\tau)}] \tag{3.5}$$

$$g(x, y, \tau) = g_o(y) + \sum_{n=1}^{\infty} \mathrm{Re}[g_n(y)e^{ni(x-\tau)}] \,. \tag{3.6}$$

This suggests that we seek solutions for ψ and p of the form

$$\psi(x, y, \tau) = \psi_o(y) + \sum_{n=1}^{\infty} \mathrm{Re}[\psi_n(y)e^{ni(x-\tau)}] \tag{3.7}$$

$$p(x, y, \tau) = p_o(y) + \sum_{n=1}^{\infty} \mathrm{Re}[p_n(y)e^{ni(x-\tau)}] \,. \tag{3.8}$$

Substituting (3.5) - (3.8) into (3.3) and (3.4), and equating the appropriate Fourier coefficients, we obtain, after some simplification (see Appendix A),

$$\psi_{o,yyy} = -f_o + R_o \{1/2 \sum_{n=1}^{\infty} \mathrm{Im}[n\psi_n\bar{\psi}_{n,y}]_{,y}\} \,, \tag{3.9}$$

$$p_{o,y} = g_o - R_o \{1/2 \sum_{n=1}^{\infty} [n^2\psi_n\bar{\psi}_n]_{,y}\} \,, \tag{3.10}$$

$$\psi_{n,yyyy} - 2n^2\psi_{n,yy} + n^2\psi_n = \pi_n + O(R_o), \quad n > 0, \tag{3.11}$$

$$p_n = \frac{1}{ni}[f_n + \psi_{n,yyy} - n^2\psi_{n,y}] + O(R_o), \quad n > 0, \tag{3.12}$$

where Im refers to the imaginary part, an overbar signifies the complex conjugate, and $\pi_n = nig_n - f_{n,y}$ $(n > 0)$.

The boundary conditions with respect to the reference frame fixed in the organism are as follows. First we impose the no-slip

condition at the wall, which requires all the Fourier components of velocity to vanish there, that is,

$$\psi_{o,y}(0) = \psi_{n,y}(0) = \psi_n(0) = 0, \qquad (n > 0). \tag{3.13}$$

Second, since we are considering an organism which is propelling itself at a constant finite speed, we require that the mean velocity remain bounded while the "AC" components of velocity vanish as $y \to \infty$. Hence,

$$\psi_{o,y}(\infty) < \infty, \ \psi_{n,y}(\infty) = \psi_n(\infty) = 0 \qquad (n > 0). \tag{3.14}$$

We note that the non-dimensional form of the condition (2.3) is

$$\begin{aligned} &f_n(y) = 0 \quad \text{for} \quad y = kY > kL, \quad n \geq 0, \quad \text{and} \\ &g_n(y) = 0 \quad \text{for} \quad y = kY > kL, \quad n \geq 0. \end{aligned} \tag{3.15}$$

Integrating equations (3.9) and (3.10) and applying the boundary conditions (3.13) and (3.14) along with the condition (3.15), we obtain for the mean velocity and pressure

$$u_o = \psi_{o,y} = \int_o^y y_1 f_o(y_1)dy_1 + y\int_y^{kL} f_o(y_1)dy_1 + R_o\{\tfrac{1}{2}\sum_{n=1}^{\infty} \mathrm{Im}[\int_o^y n\psi_n\bar{\psi}_{n,y}dy_1]\} \tag{3.16}$$

$$p_o = p_\infty + \int_o^y g_o(y_1)dy_1 - R_o\{\tfrac{1}{2}\sum_{n=1}^{\infty} n^2\psi_n\bar{\psi}_n\}, \tag{3.17}$$

where p_∞ is a constant. Note that as a result of (3.15), the zeroth order terms (in R_o) of u_o and p_o are constant for $y = kY > kL$.

As can be seen from the integrands of (3.16), the chief source of the velocity at infinity, which corresponds to the speed of propulsion, is the distribution of the mean x-component of body force within the cilia layer. The terms of order R_o come from the coupling of the "AC" velocities in the nonlinear inertial terms of the fundamental equations. The solution to (3.11) subject to (3.13), (3.14) and (3.15) (see Appendix B) is

$$\psi_n = \frac{1}{4n^2}\left[a_n(y)e^{ny} + \beta_n(y)e^{-ny}\right] + O(R_o), \quad \text{where} \tag{3.18}$$

$$a_n(y) = \int_{kL}^{y} (y-y_1 - \frac{1}{n})e^{-ny_1}\ \pi_n\, dy_1, \tag{3.19}$$

$$\beta_n(y) = \int_{o}^{y} (y-y_1 + \frac{1}{n})e^{ny_1}\ \pi_n dy_1 - \int_{o}^{kL} (y+y_1+2nyy_1+\frac{1}{n})e^{-ny_1}\ \pi_n dy_1. \tag{3.20}$$

The harmonic x and y velocities, $u_n = \mathrm{Re}\left[\psi_{n'y}e^{ni(x-\tau)}\right]$ and $v_n = -\mathrm{Re}\left[ni\psi_n e^{ni(x-\tau)}\right]$, $n > 0$, are given by

$$u_n = \mathrm{Re}\left\{\frac{1}{4n^2}\left[(a_{n,y} + na_n)e^{n(y+i\varphi)} + (\beta_{n,y} - n\beta_n)e^{-n(y-i\varphi)}\right]\right\} + O(R_o), \tag{3.21}$$

$$v_n = -\mathrm{Re}\left\{\frac{i}{4n}\left[a_n e^{n(y+i\varphi)} + \beta_n e^{-n(y-i\varphi)}\right]\right\} + O(R_o), \tag{3.22}$$

where $\varphi = x-\tau$. Note from (3.15) and (3.19) that a_n and $a_{n,y}$ vanish for $y = kY > kL$, so that the harmonic velocities decay like e^{-nkY}. The dimensional velocities U_n and V_n are obtained by simply multiplying u_n and v_n by $c = \omega/k$, the wave speed. The solution for the

harmonic pressure coefficients may be determined from (3. 12) and (3. 18) directly.

Finally we observe that for the cilia layer to be self-propelling, the condition of zero mean longitudinal force acting on the organism can be expressed by

$$\mu \frac{dU_o(0)}{dY} = \int_o^L F_o(Y_1)dY_1, \tag{3.23}$$

where $\mu = \rho\nu$ is the dynamic viscosity coefficient; the mean shearing force exerted by the fluid on the wall balances the mean force per unit area of the organism's surface due to the reaction of the fluid to the ciliary body force field. It is of interest to note that the present solution, given by (3. 16) - (3. 20), satisfies condition (3. 23) required for self-propulsion when the bulk force $\underline{F}$ of ciliary layer is regarded as known. This is in effect a consequence of the boundary condition imposed at infinity, as Taylor (1951) pointed out. To an observer in a frame fixed with the fluid at infinity (the lab frame), the organism is moving with a constant velocity and hence, by conservation of momentum, must have zero net force acting on it.

4. Force exerted by a cilium

In the preceding section the solution to the fluid mechanical problem was given as if the body force field $\underline{F}$ were known a priori. Since in practice this is not the case, we need to develop a means of determining $\underline{F}$. As an initial step in this regard, we consider the force exerted on the fluid by a single cilium.

In order to calculate the viscous force exerted by an elongated cylindrical body moving through a viscous fluid, it is convenient to utilize the simple approximations of slender-body resistive theory. If the tangential and normal velocities relative to the primary flow of a cylindrical body element of length ds are $\underline{V}_s$ and $\underline{V}_n$ respectively, the tangential force exerted by the body element on the viscous fluid will be $d\underline{F}_s = C_s \underline{V}_s \, ds$ with a similar expression for the normal force $d\underline{F}_n = C_n \underline{V}_n \, ds$, where C_s and C_n are the corresponding resistive force coefficients.

The expressions for the force coefficients have received considerable attention by several authors. The original expressions given by Gray and Hancock (1955) were for an infinitely long circular cylindrical filament along which planar waves of lateral displacement are propagated in an unbounded fluid. Cox (1970) developed slightly modified coefficients to account for other simple shapes. Recent work by Katz and Blake (1974) have yielded improved coefficients for slender bodies undergoing small amplitude normal motions near a wall. For the purposes of the present investigation, however, initially, the force coefficients developed by Chwang and Wu (1974) for a very thin ellipsoid of semi-major axis $\frac{1}{2}L$, and semi-minor axis r_o are used.

These were found to be

$$C_n = \frac{4\pi\mu}{\ln(L/r_o) + \frac{1}{2}} \quad \text{and} \quad C_s = \frac{2\pi\mu}{\ln(L/r_o) - \frac{1}{2}}. \tag{4.1}$$

We may describe the motion of a single cilium with base fixed at the origin by a parametric position vector $\underline{\xi}(s,t)$ specifying the position of the element ds of the cilium identified by the arc length s at time t (see Figure 3). The force exerted by the element ds on the fluid is given by

$$d\underline{F}_c = d\underline{F}_s + d\underline{F}_n \tag{4.2}$$

$$= C_s \underline{V}_s\, ds + C_n \underline{V}_n\, ds \tag{4.3}$$

$$= C_s\{[(\underline{\xi}_{,t} - \underline{U}) \cdot \underline{e}_s]\underline{e}_s + \gamma[(\underline{\xi}_{,t} - \underline{U}) \cdot \underline{e}_n]\underline{e}_n\}\, ds, \tag{4.4}$$

where $\underline{U}$ is the local primary flow velocity, $\gamma = C_n/C_s$, $\underline{e}_s$ is a unit vector tangential to the longitudinal curve of the cilium centroid, and $\underline{e}_n$ is a unit vector normal to $\underline{e}_s$ lying in the plane formed by $\underline{\xi}_{,t} - \underline{U}$ and $\underline{e}_s$. From elementary calculus it is easily found that $\underline{e}_s = \underline{\xi}_{,s}$ and

$$\underline{e}_n = [\underline{V} - (\underline{V} \cdot \underline{\xi}_{,s})\,\underline{\xi}_{,s}] / |\underline{V} - (\underline{V} \cdot \underline{\xi}_{,s})\underline{\xi}_{,s}| \tag{4.5}$$

where $\underline{V} = \underline{\xi}_{,t} - \underline{U}$. Substituting (4.5) in (4.4) yields

$$d\underline{F}_c = C_s[\gamma(\underline{\xi}_{,t} - \underline{U}) + (1-\gamma)\underline{\xi}_{,s}(\underline{\xi}_{,t} - \underline{U}) \cdot \underline{\xi}_{,s}]\, ds. \tag{4.6}$$

We are thus left with the task of evaluating $\underline{F}_c$ and then converting it to the body force field.

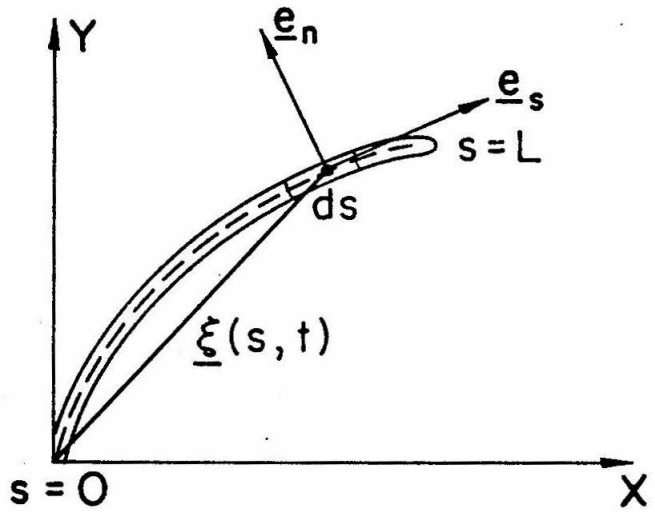

Fig. 3 Description of the motion of a cilium by a parametric position vector.

5. Determination of the body force field

In order to apply the resistive theory in determining the body force field $\underline{F}$, two difficulties must be overcome. Equation (4. 6) describes the force exerted by an element as a function of its arc length s. It is convenient to convert this Lagrangian description of the force to Eulerian coordinates (i. e. to express the force as a function of X and Y). In addition, the force exerted by an element depends upon the local fluid velocity, which is initially unknown. Both of these features suggest a numerical iteration approach.

In the following paragraphs the main elements of the numerical scheme will be described briefly. From (2. 1) it follows that

$$\underline{F}_o = \frac{1}{\lambda}\int_o^{\lambda} \underline{F}(X, Y, t_o)dX, \quad \underline{F}_n = \frac{2}{\lambda}\int_o^{\lambda} \underline{F}(X, Y, t_o)\, e^{-ni\phi}dX \quad (n \geqslant 1)\,. \tag{5. 1}$$

This implies that if the body force field were known over one wavelength for some (arbitrary) fixed time t_o, then all the force coefficients could be determined. In order to accomplish this for a given ciliary beat pattern, an analytical representation for $\underline{\xi}(s,t)$ can be determined using a finite Fourier series-least square procedure. (For the details of this procedure see Blake, 1972). Thus the movement of a single cilium is given by

$$\underline{\xi}(s,t) = \tfrac{1}{2}\,\underline{a}_o(s) + \sum_{n=1}^{N} \underline{a}_n(s)\cos n\omega t + \underline{b}_n(s)\sin n\omega t, \tag{5. 2}$$

where $\underline{a}_n(s) = \sum_{m=1}^{M} \underline{A}_{mn} s^m$, $\underline{b}_n(s) = \sum_{m=1}^{M} \underline{B}_{mn} s^m$, with $\underline{A}_{mn}$ and

$\underline{B}_{mn}$ being constant vectors, N is the order of the Fourier series, and M is the degree of the least squares polynomial expansion used.

Once $\underline{\xi}(s,t)$ is determined, an initial body force field can be established via a "pigeon-hole" algorithm. Using (5. 2), the cilia are numerically distributed over one wavelength at a fixed time t_o and each cilium is broken up into a finite number of segments. The Eulerian location of and the force exerted by each segment are then determined and stored (i. e. "pigeon-holed"). The force is evaluated using (4. 6) initially with $\underline{U}$, the local fluid velocity, equal to zero. The approximation is made that the force exerted by each segment is located at the midpoint of that segment, so that the force field can be represented by the expression

$$\underline{F}(X, Y, t_o) = \frac{1}{b} \sum_{j=1}^{J} \underline{f}_j \delta(X-X_j)\, \delta(Y-Y_j), \qquad (5.3)$$

where $\underline{f}_j$ is the force exerted by the j-th ciliary segment whose midpoint is located at (X_j, Y_j) and J is the total number of segments in one wavelength. The factor 1/b accounts for the averaging in the Z direction.

Calculations of the body force field can then be carried out by iteration. Equation (5. 3) is used in (5. 1) to determine the Fourier force coefficients $\underline{F}_n$ $(n \geqslant 0)$. These coefficients, after non-dimensionalization, are then used in (3. 16) and (3. 18) to determine a new primary velocity field $\underline{U}$ in which the cilia are assumed to be immersed. This velocity field is used anew in the pigeon-hole algorithm to determine a new $\underline{F}(X, Y, t_o)$ by computing new $\underline{f}_j$'s. The

iterative process is thus repeated until the $\underline{f}_j$'s, and hence the velocity field $\underline{U}$, converges.

6. Results for Paramecium and Opalina

Calculations have been carried out on data obtained for Opalina ranarum and Paramecium multimicronucleatum. Opalina is a flat disc shaped ciliated protozoon found in frogs, while Paramecium is a prolate spheroidal shaped ciliate commonly found in stagnant water. Although these two organisms have been observed to have somewhat three-dimensional beat patterns, they were chosen because of the availability of the necessary data and for comparison with previous theoretical work. The raw planar beat patterns were taken from Sleigh (1968) and Tables 3 and 4 give the calculated Fourier series - least squares coefficients (see (5. 2)) with $M = N = 3$ for Opalina and $M = N = 4$ for Paramecium. Using these coefficients, we present computer plots of the beat patterns in Figure 4. The metachrony of Opalina is symplectic (Sleigh, 1968), while Paramecium was regarded as exhibiting antiplectic metachrony, although it recently has been reported to be dexioplectic (Machemer, 1972b).

In order to display the harmonic X-velocity components, it is convenient to write them in the form

$$U_n = Q_n \cos(n\phi + \theta_n), \quad (n \geq 1), \quad \text{where} \tag{4. 1}$$

$$Q_n = c \, | \psi_{n,y} | \, , \text{ and} \tag{4. 2}$$

$$\theta_n = \tan^{-1} [\mathrm{Im}(\psi_{n,y})/\mathrm{Re}(\psi_{n,y})] \tag{4. 3}$$

For a given value of Y, Q_n is the amplitude of the nth harmonic X-velocity component, while θ_n is the phase of the motion. This phase

TABLE 3

Fourier series - least squares coefficients for the beat pattern of Opalina drawn by Sleigh (1968).

$\underline{A}_{mn}$

m \ n	0	1	2	3
1	1.5170	-0.1957	0.0732	0.0838
	1.1290	0.3079	-0.1510	-0.1060
2	-0.0886	-0.4235	-0.5698	-0.3278
	-0.4102	0.4428	0.7006	0.3409
3	0.1248	0.3126	0.3866	0.2143
	0.0298	0.3903	0.4920	0.2007

$\underline{B}_{mn}$

m \ n	0	1	2	3
1	.....	0.2801	0.2157	0.0961
	.....	-0.2855	-0.1250	0.0225
2	.....	-0.5157	-0.3445	-0.0548
	.....	0.7350	0.2241	-0.3343
3	.....	0.2163	0.1105	-0.0197
	.....	-0.2740	0.0386	0.3104

Note: The length of the cilium has been normalized to 1. Upper and lower coefficients in each box correspond to X and Y components of cilium position vector respectively.

TABLE 4

Fourier series - least squares coefficients for the beat pattern of Paramecium drawn by Sleigh (1968).

$\underline{A}_{mn}$

m \ n	0	1	2	3	4
1	-1.2580	0.1458	-0.3606	0.0663	0.0534
	1.5270	0.1795	-0.1878	-0.0074	-0.0063
2	1.3528	-0.1122	0.0466	-0.2385	-0.2774
	-0.4827	-0.7740	1.0896	-0.1997	-0.5204
3	-0.0920	-1.9370	0.8160	0.3980	0.4446
	0.6804	1.4682	1.7339	0.2671	0.1937
4	0.0928	1.4216	-0.7118	-0.2339	-0.2340
	-0.4941	-0.6901	0.8636	-0.1165	-0.0924

$\underline{B}_{mn}$

m \ n	0	1	2	3	4
1	.....	0.0565	0.3987	-0.0502	0.0851
	.....	0.1734	-0.0863	0.0406	-0.0085
2	.....	2.5308	-2.5708	0.1122	-0.3483
	.....	-0.2149	0.7584	-0.0888	0.0421
3	.....	3.2568	4.2679	-0.2352	0.5374
	.....	-0.2868	0.9381	0.1863	-0.0492
4	.....	1.0828	-2.1502	0.1243	-0.2599
	.....	0.3610	0.3697	-0.0867	0.0136

Note: The length of the cilium has been normalized to 1. Upper and lower coefficients in each box correspond to X and Y component of cilium position vector respectively.

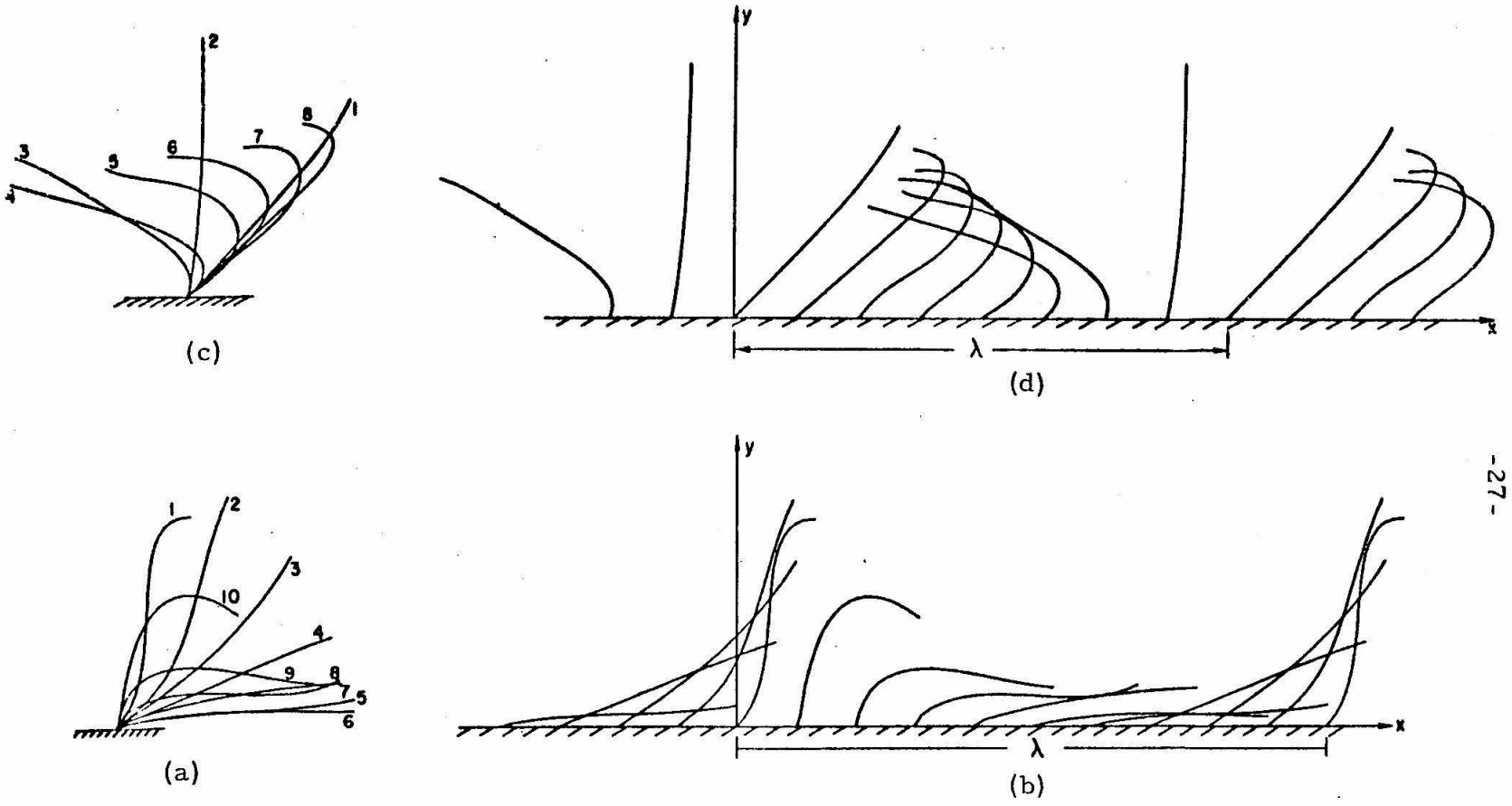

Fig. 4 Plots of the analytical representation of the beat patterns for Opalina (a,b) and Paramecium (c, d). Numbers indicate successive equal time increments of the beat cycle. The movement of an individual cilium is shown in (a) and (c), while (b) and (d) represent a "snapshot" of the cilia at $t = t_o$.

is such that U_n is at a maximum and in the same direction as the mean flow when $\phi = (2\ell\pi - \theta_n)/n$, while U_n is at a maximum and opposes the mean flow when $\phi = [(2\ell - 1)\pi - \theta_n]/n$, where ℓ is an integer.

In performing the computations, besides the basic beat pattern, it was necessary to specify the three-dimensionless parameters ka, kb, and kL. The values of the parameters were chosen to be consistent with the consensus of experimental observations (see Tables 1 and 2). The values used for ka and kb were 0.63 and 0.13 for Opalina and 0.80 and 1.60 for Paramecium. Two values of the amplitude parameters kL, to which the computations were the most sensitive, were used for each organism, these being 1.25 and 2.50 for Opalina and 3.00 and 6.00 for Paramecium. Because of the apparent rapid decay of the higher harmonics and for computational efficiency, only the first harmonic was retained in computing the local velocity field U in three cases, however, the second harmonic was included for Paramecium with kL = 3.00.

Figures 5 and 6 show the velocity profiles for U_o, the mean fluid velocity parallel to the wall, for Opalina and Paramecium respectively. Also plotted are the profiles given by Blake (1972) (dashed curve). The velocities at infinity, U^∞/c, which correspond to the velocities of propulsion, are seen to agree quite well with the observed values of 0.5 - 1.5 for Opalina and 1 - 4 for Paramecium (Brennen, 1974). Blake's calculations were made with the quantity (ka) (kb) equal to 0.04 for Opalina and 0.0025 for Paramecium (both far below the reported values) so that a direct comparison is difficult.

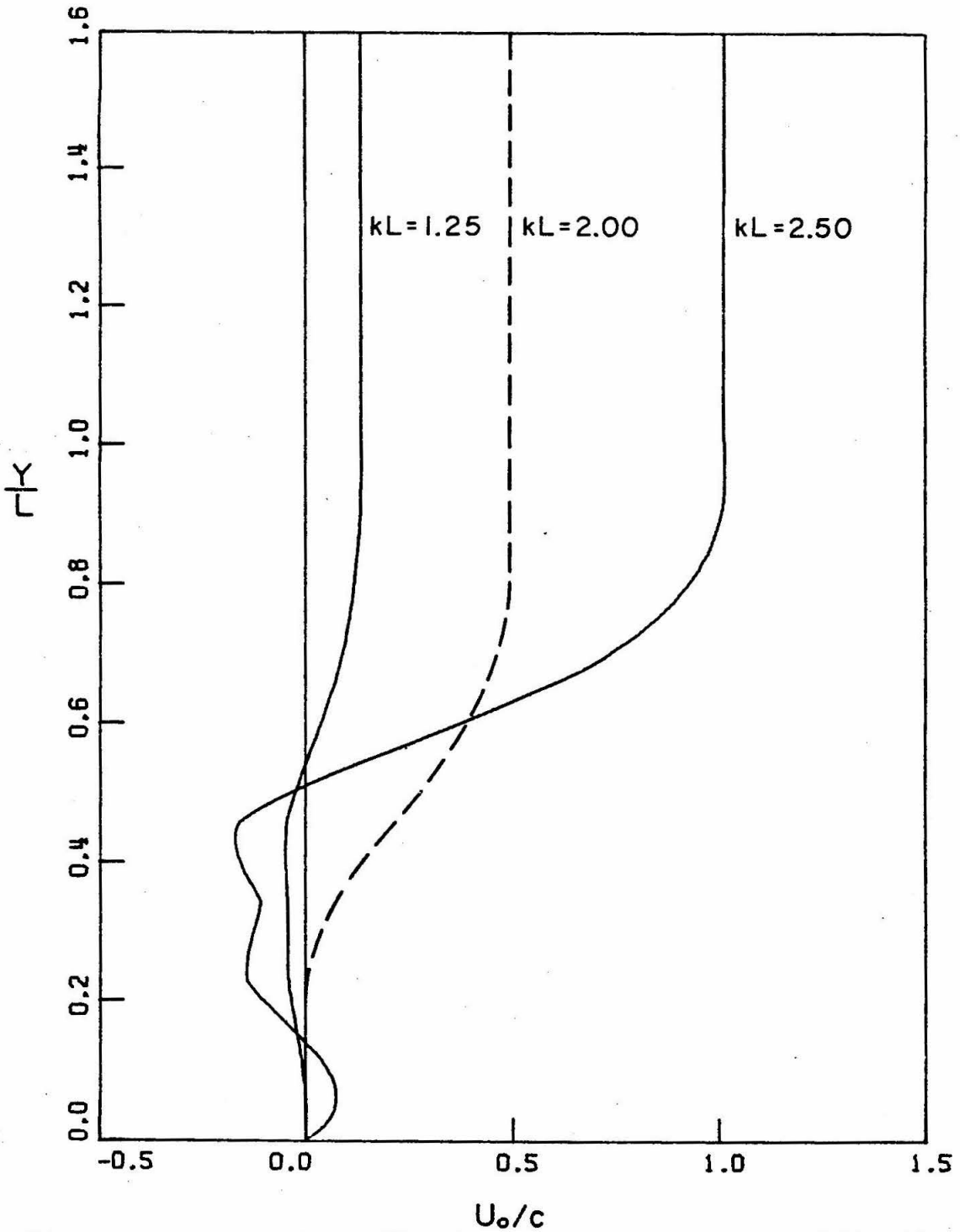

Fig. 5 Mean velocity profiles for Opalina with ka=.63 and kb=.13 . Dashed curve is from Blake (1972) for which (ka)(kb)=.04 .

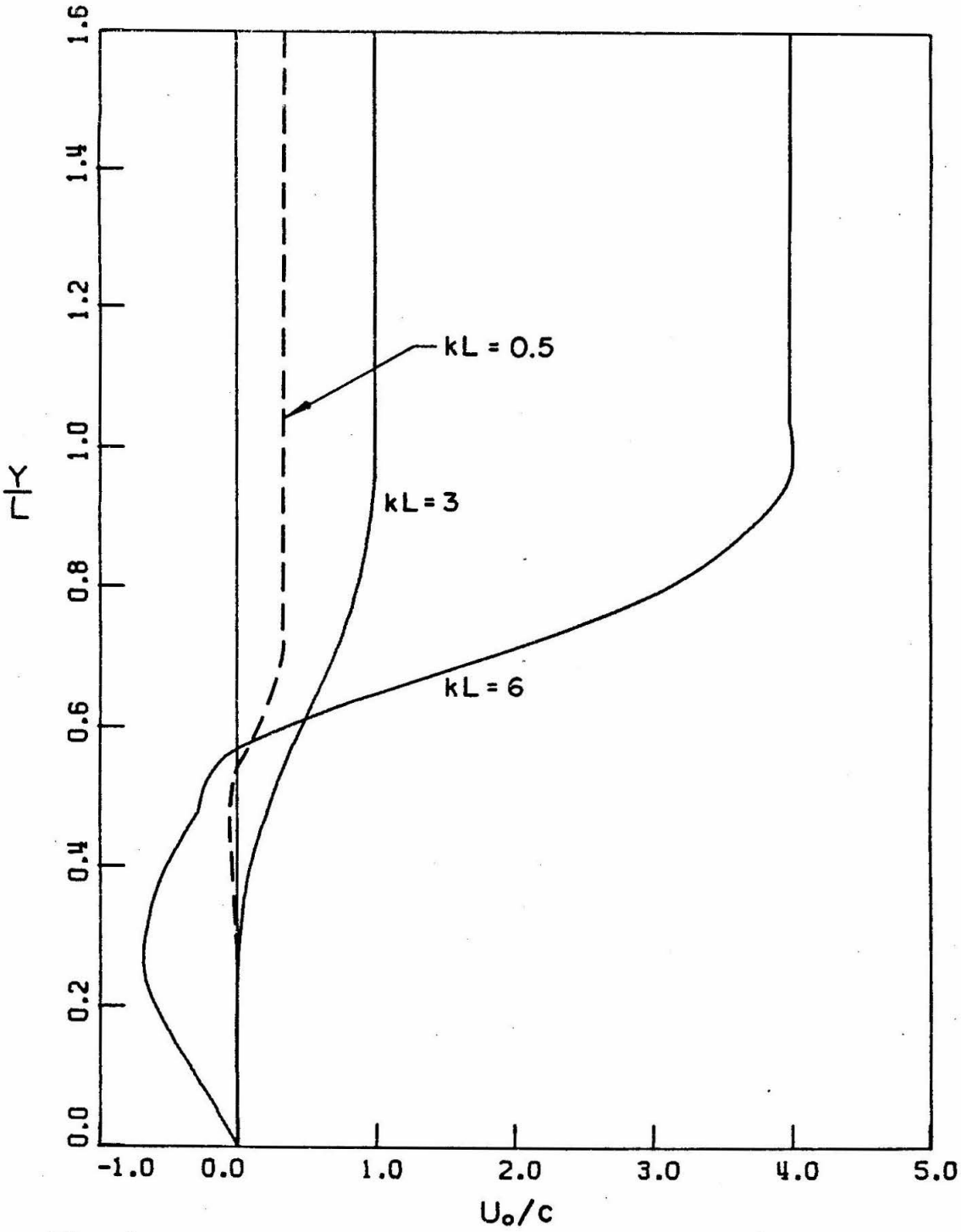

Fig. 6 Mean velocity profiles for Paramecium with ka = 0.80 and kb = 1.60. Dashed curve is from Blake (1972) for which (ka)(kb) = .00025.

While Blake's results indicate a slight backflow for only the antiplectic case, the present study indicates a backflow in the lower half of the cilia layer for both Opalina and Paramecium (for kL = 6).

Figure 7 shows the amplitude of the first harmonic velocity component U_1 for Opalina. The largest oscillatory velocities appear to occur at Y/L = 6 and are more than twice the mean flow in magnitude. In Figure 8 the amplitudes of U_1 for kL equal 3 and 6 and U_2 for kL equal 3 are shown for Paramecium. The largest oscillatory velocities occur in the upper part of the cilia layer and are about the same magnitude as the mean flow. Note that for kL = 3 the amplitude of U_2 is half that of U_1.

The corresponding θ_n's for Figures 7 and 8 are shown in Figures 9 and 10 respectively. The origin and the value of t_o (see section 5) were chosen so that $\phi = 0$ corresponds to a metachronal wave peak under which the cilia are in the effective stroke. This is illustrated in Figures 4b, d which can be regarded as snapshots of the cilia at $t = t_o$. For Opalina at Y/L = 0.5 and $\phi = 0$, $U_1/Q_1 = \cos(\theta_1)$ equals approximately 1 for kL = 1.25 and 0 for kL = 2.5. This means that U_1 is somewhat in the same direction as the mean flow in the vicinity of the cilia performing the effective stroke. However, above Y/L = 0.5 U_1 progressively tends to oppose the mean flow. For Paramecium however, at Y/L = 0.5 and $\phi = 0$, U_1/Q_1 equals -1 (approximately) for both kL values. Thus, in this case, U_1 tends to oppose the mean flow in the vicinity of the effective stroke. It is also seen that U_2 (for kL = 3) is in the same direction as the mean flow near the effective stroke ($\phi = 0$) for much of the cilia layer.

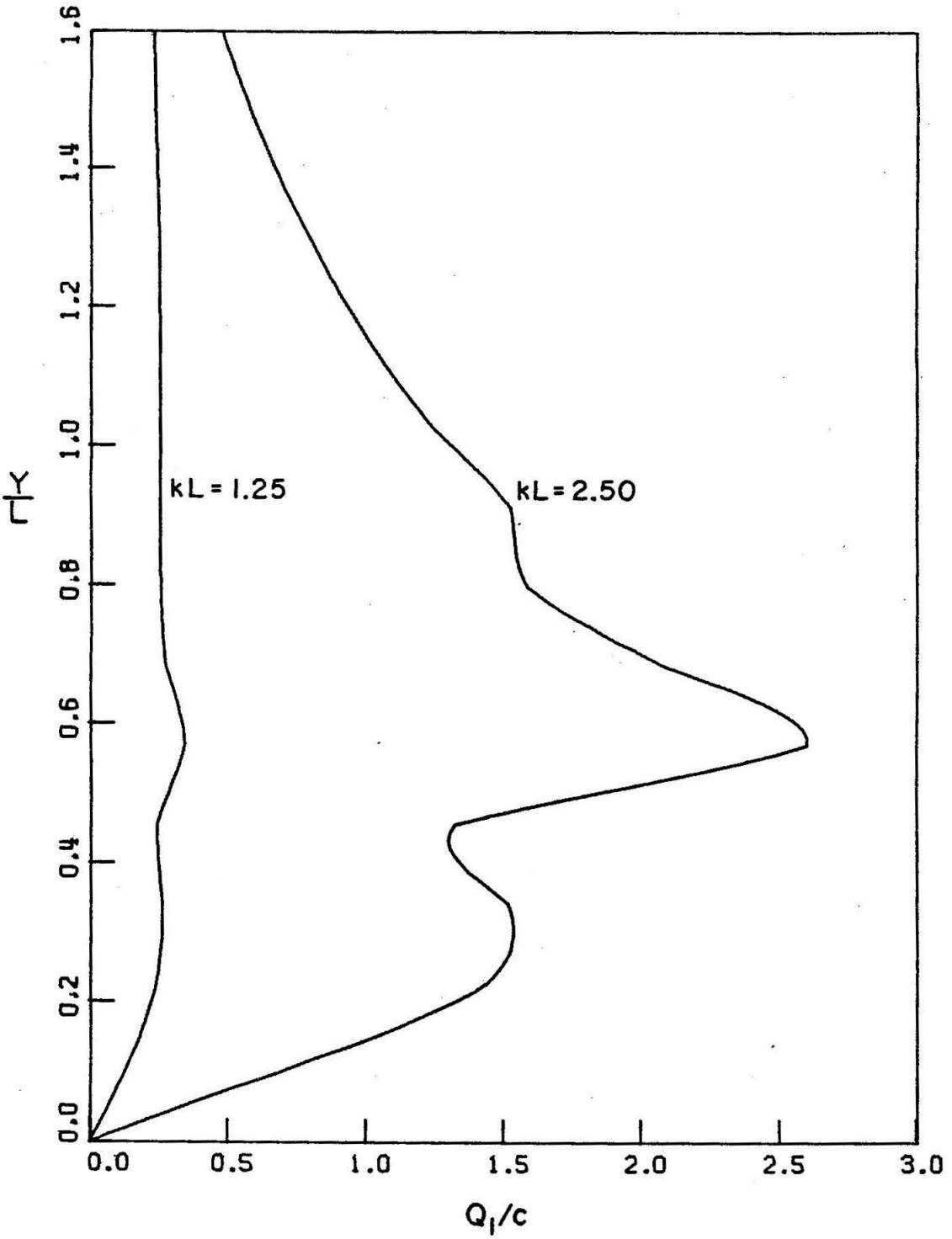

Fig. 7 Amplitude profile for the first harmonic X-velocity component for Opalina with ka=.63 and kb=.13 .

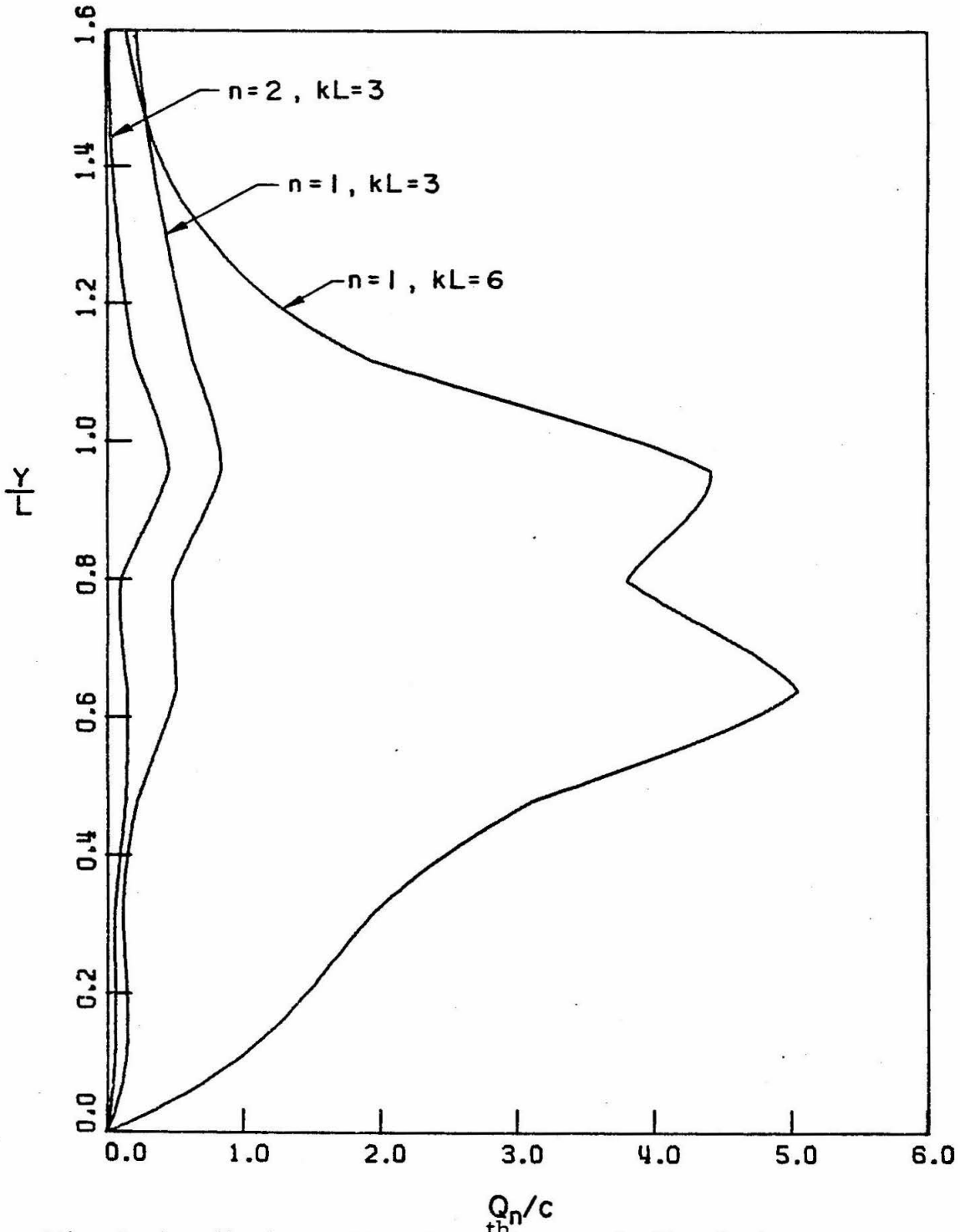

Fig. 8 Amplitude profiles for n^{th} harmonic X-velocity components for Paramecium with ka=.80 and kb=1.60 .

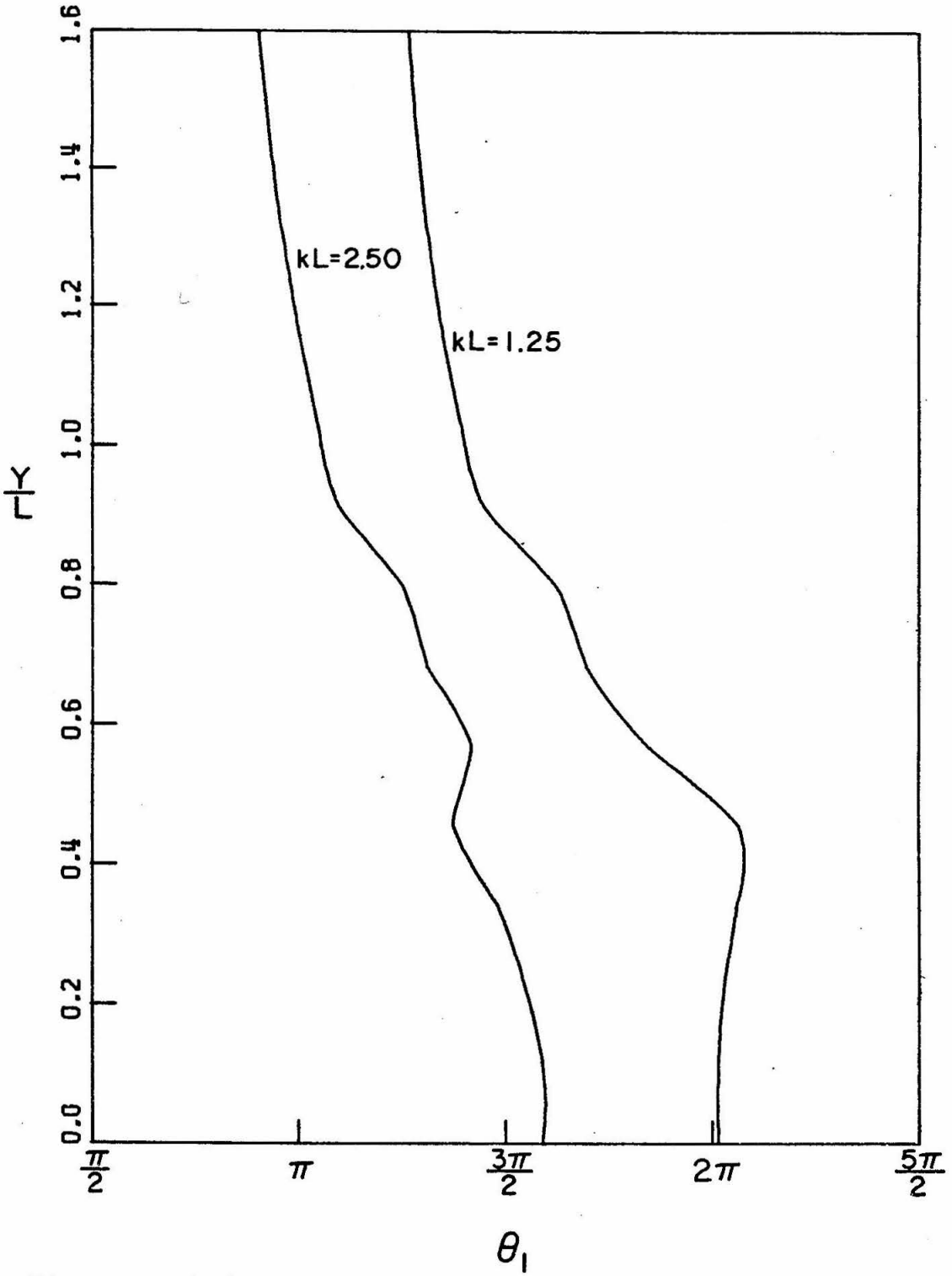

Fig. 9 Variation of θ_1, the phase of the first harmonic X-velocity component, with Y/L for Opalina.

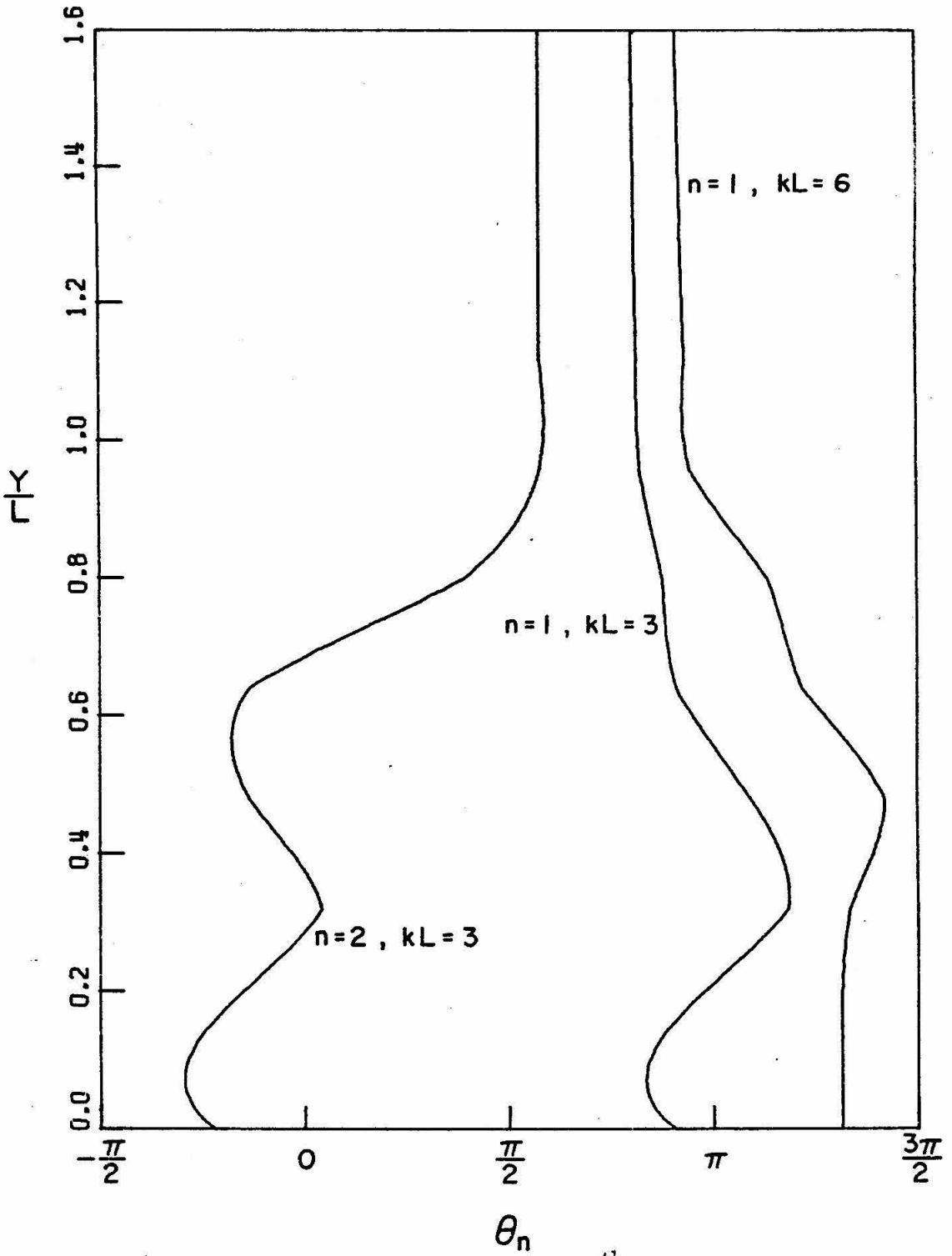

Fig. 10 Variation of θ_n, the phase of the n^{th} harmonic X-velocity component, with Y/L for Paramecium .

7. Energy expenditure by a cilium

Once the final velocity field $\underline{U}$ has been determined, the rate of energy expenditure by an individual cilium can be calculated. The rate of working of a single cilium, $\dot{E}_c$, is the sum of the rates of working of the cilium elements. Therefore we may write

$$\dot{E}_c(t) = \int_0^L [\underline{\xi}_{,t}(s,t) - \underline{U}] \cdot \frac{d\underline{F}_c}{ds}(s,t)ds, \qquad (7.1)$$

where $\underline{U}$ is regarded as a function of s and t. This integral was carried out numerically for Opalina and Paramecium using the final $\underline{f}_j$'s (see section 5) obtained in the computations of the previous section. In specifying $\underline{U}$, in addition to the mean flow, both the first and second harmonics were retained.

Figures 11 and 12 show the power expended by a cilium over one beat cycle for Paramecium and Opalina respectively. The power, $\dot{E}_c$, on the vertical axis has been non-dimensionalized by the quantity $\mu c^2/k$. The rate of working for Paramecium is greatest during the effective stroke, while Opalina has two peaks of power output, one during the effective stroke and one during the latter part of the return stroke. Note that the power expenditure is very sensitive to the amplitude parameter kL; the upper curve in each figure, which corresponds to the higher kL value, has been scaled by a factor of 10^{-1}.

Also shown in Figures 11 and 12 are the energy expenditure curves computed using only the mean flow for Paramecium with kL = 6 and for Opalina with kL = 1.25 (labelled NHARM = 0).

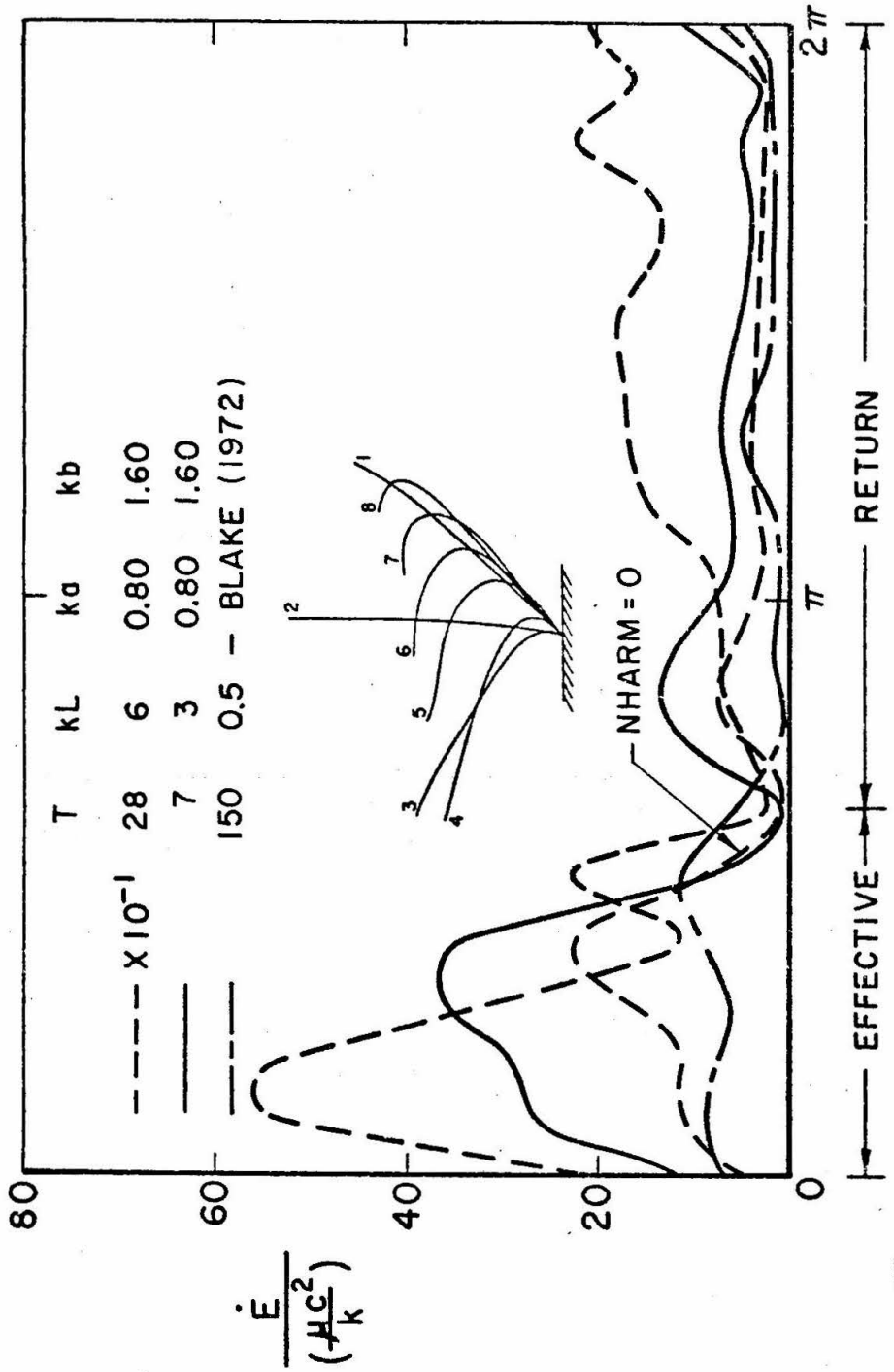

Fig. 11 The power expended by a cilium over one beat cycle for Paramecium.

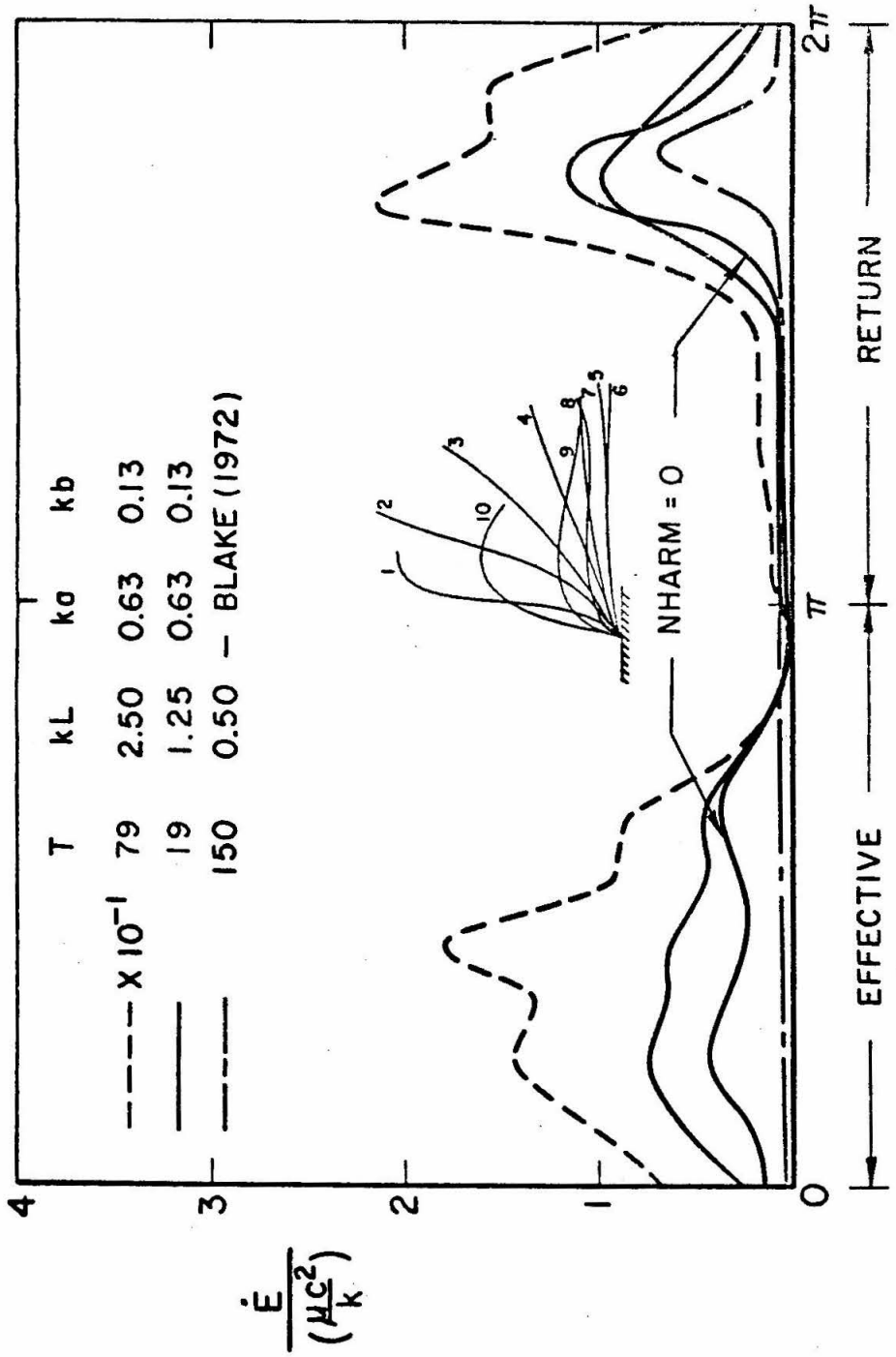

Fig. 12 The power expended by a cilium over one beat cycle for Opalina.

It is seen that when the oscillatory velocities are neglected, the energy expenditure over one beat cycle is substantially less than that obtained with the oscillatory components included. The corresponding curves obtained from the analysis of Blake (1972) are also indicated on the figures. In the present notation, the parameter T used by Blake is given by $C_s(kL)^2/[\mu(ka)(kb)]$. Because of the discrepancies in the values of T and kL used, a comparison of the results is difficult.

Finally it is of interest to estimate the actual work done, W_c, by a cilium against viscosity over one beat cycle, which is given by the area under the curves of Figures 11 and 12 times the quantity $\mu c^2/k$. For Opalina this quantity is about 35×10^{-10} ergs/sec, while for Paramecium it is about 92×10^{-10} ergs/sec. Therefore it is found that for Opalina with $kL = 2.5$, $W_c = 1 \times 10^{-8}$ ergs and for Paramecium with $kL = 3$, $W_c = 0.4 \times 10^{-8}$ ergs. These values are in agreement with an estimate of the work done by a component cilium of the compound abfrontal cilium of Mytilus obtained from the experimental work of Baba and Hiramoto (1970). Hiramoto (1974) estimates that the work done by a single component cilium is 1×10^{-8} erg beat^{-1}. Furthermore, Sleigh and Holwill (1969), using a biochemical approach based upon the number of ATP molecules de-phosphorylated per beat, estimate that the amount of energy available for movement in one beat of a cilium was 2.4×10^{-8} ergs for Sabellaria and 3.8×10^{-8} ergs for Mytilus. These estimates, although applied to different organisms, are seen to be consistent with the present theory.

8. Conclusions and discussion

The concept of replacing the discrete cilia ensemble mathematically by a layer of body force leads to a reasonably successful model for ciliary propulsion. The principal advantages of this approach are that it allows for the large amplitude movement of cilia and takes into account the oscillatory aspects of the flow.

When applied to Opalina and Paramecium, a good agreement is found between theoretically predicted and experimentally observed velocities of propulsion. The amplitude of the oscillatory velocities is found to be of the same order of magnitude as the mean flow within the layer and to decay exponentially outside the cilia layer.

The energy expenditure by a single cilium over one beat cycle is found to be very sensitive to the amplitude of the ciliary movement and to be significantly greater than previous theoretical estimates which neglected the oscillatory components of the flow field. The work done by an individual cilium against viscosity during one beat cycle is found to be consistent with experimental and biochemical estimates.

The principal limitation of the model is due to the geometry employed. The main objection is that an infinite flat sheet model is limited in its capacity to assess the effect of the finite three-dimensional shape of the organism. While this criticism is valid, because of the mathematical complexities involved, it seems likely that geometrically simplified models will contribute most to our detailed knowledge of ciliary propulsion. Furthermore it has been demonstrated that infinite models may be profitably employed as local approximations for finite geometries (Blake, 1973; Brennen, 1974).

A second limitation of the present approach is with regard to the approximations of the slender-body resistive theory used. The problem of calculating the force exerted by a slender body moving in a given primary flow field in close proximity to many neighboring bodies and in the vicinity of a wall is an enormous one. It is felt that the present resistive theory approach provides a reasonable alternative to the task of rigorously considering these complications. The effect of the wall is taken into account by imposing the no-slip condition upon the flow, while the influence of the neighboring cilia elements is effectively represented in the local primary flow field. While the resistive coefficients employed, C_n and C_s, were developed for a slender body immersed in a uniform primary flow, it is reasonable to expect that these coefficients would be useful approximations for non-uniform primary flows. In this regard the work by Cox (1971) on a slender body immersed in a primary shear flow indicates that more refined coefficients would not alter the results greatly.

Appendix A

Derivation of equations (3. 9) - (3. 12)

Equations (3. 9) - (3. 12) are obtained from the substitution of the Fourier expansions for ψ, p, f and g given by (3. 5) - (3. 8) into the equations of motion (3. 3) and (3. 4). We consider the linear and nonlinear terms separately. The linear terms needed are

$$f = f_o + \sum_{n=1}^{\infty} \mathrm{Re}(f_n e^{ni\varphi}), \quad \text{where } \varphi = x-\tau, \tag{A. 1}$$

$$g = g_o + \sum_{n=1}^{\infty} \mathrm{Re}(g_n e^{ni\varphi}), \tag{A. 2}$$

$$p_{,x} = \sum_{n=1}^{\infty} \mathrm{Re}(nip_n e^{ni\varphi}), \tag{A. 3}$$

$$p_{,y} = p_{o,y} + \sum_{n=1}^{\infty} \mathrm{Re}(p_{n,y} e^{ni\varphi}), \tag{A. 4}$$

$$\psi_{,x\tau} = \sum_{n=1}^{\infty} \mathrm{Re}(n^2\psi_n e^{ni\varphi}), \tag{A. 5}$$

$$\psi_{,y\tau} = -\sum_{n=1}^{\infty} \mathrm{Re}(ni\psi_{n,y} e^{ni\varphi}), \tag{A. 6}$$

$$\nabla^2\psi_{,y} = \psi_{o,yyy} + \sum_{n=1}^{\infty} \mathrm{Re}[\psi_{n,yyy} - n^2\psi_{n,y})e^{ni\varphi}], \text{ and} \tag{A. 7}$$

$$\nabla^2\psi_{,x} = \sum_{n=1}^{\infty} \mathrm{Re}[(ni\psi_{n,yy} - n^3 i\psi_n)e^{ni\varphi}]. \tag{A. 8}$$

Before considering the nonlinear terms, we note that if z_1 and z_2 are two complex numbers and m and n are integers, then

$$\mathrm{Re}(z_1 e^{mi\varphi})\mathrm{Re}(z_2 e^{ni\varphi}) = \tfrac{1}{2}\,\mathrm{Re}(z_1\bar{z}_2 e^{(m-n)i\varphi} + z_1 z_2 e^{(m+n)i\varphi}) , \tag{A. 9}$$

Therefore it is easily seen that

$$\psi_{,y}\psi_{,xy} = -\tfrac{1}{2}\sum_{n=1}^{\infty}\mathrm{Re}(ni\psi_{n,y}\bar{\psi}_{n,y}) + \text{AC terms} , \tag{A. 10}$$

$$\psi_{,x}\psi_{,yy} = \tfrac{1}{2}\sum_{n=1}^{\infty}\mathrm{Re}(ni\psi_{n}\bar{\psi}_{n,yy}) + \text{AC terms} , \tag{A. 11}$$

$$\psi_{,y}\psi_{,xx} = -\tfrac{1}{2}\sum_{n=1}^{\infty}\mathrm{Re}(n^2\psi_{n,y}\bar{\psi}_{n}) + \text{AC terms} , \tag{A. 12}$$

$$\psi_{,x}\psi_{,xy} = \tfrac{1}{2}\sum_{n=1}^{\infty}\mathrm{Re}(n^2\psi_{n}\bar{\psi}_{n,y}) + \text{AC terms} . \tag{A. 13}$$

Using (A. 10) - (A. 13), we easily determine the needed nonlinear terms to be

$$\begin{aligned}\psi_{,y}\psi_{,xy} - \psi_{,x}\psi_{,yy} &= -\tfrac{1}{2}\sum_{n=1}^{\infty}\mathrm{Re}[ni(\psi_{n,y}\bar{\psi}_{n,y} + \psi_{n}\bar{\psi}_{n,yy})] \\ &\quad + \text{AC terms} \qquad\qquad (A.\ 14)\\ &= -\tfrac{1}{2}\sum_{n=1}^{\infty}\mathrm{Re}[ni(\psi_{n}\bar{\psi}_{n,y})_{,y}] + \text{AC terms} \\ &= \tfrac{1}{2}\sum_{n=1}^{\infty}\mathrm{Im}[n(\psi_{n}\bar{\psi}_{n,y})_{,y}] + \text{AC terms, and}\end{aligned}$$

$$\psi_{,y}\psi_{,xx} - \psi_{,x}\psi_{,xy} = -\tfrac{1}{2}\sum_{n=1}^{\infty} \mathrm{Re}[n^2(\psi_{n,y}\bar{\psi}_n + \psi_n\bar{\psi}_{n,y})] + \text{AC terms}$$

$$= -\tfrac{1}{2}\sum_{n=1}^{\infty} \mathrm{Re}[n^2(\psi_n\bar{\psi}_n)_{,y}] + \text{AC terms}$$

$$= -\tfrac{1}{2}\sum_{n=1}^{\infty} n^2(\psi_n\bar{\psi}_n)_{,y} + \text{AC terms} . \qquad \text{(A. 15)}$$

Upon substituting (A. 1) - (A. 8), (A. 14), and (A. 15) into (3. 3) and (3. 4) and collecting terms, we find that

$$0 = f_o + \psi_{o,yyy} - R_o[\tfrac{1}{2}\sum_{n=1}^{\infty} \mathrm{Im}(n\psi_n\bar{\psi}_{n,y})_{,y}]$$

$$+ \sum_{n=1}^{\infty} \mathrm{Re}\{[(f_n - nip_n + \psi_{n,yyy} - n^2\psi_{n,y}) + R_o(ni\psi_{n,y})]e^{ni\varphi}\}$$

$$+ R_o(\text{AC terms}), \quad \text{and} \qquad \text{(A. 16)}$$

$$0 = g_o - p_{o,y} - R_o[\tfrac{1}{2}\sum_{n=1}^{\infty} (n^2\psi_n\bar{\psi}_n)_{,y}]$$

$$+ \sum_{n=1}^{\infty} \mathrm{Re}\{[(g_n - p_{n,y} - ni\psi_{n,yy} + n^3i\psi_n) + R_o(n^2\psi_n)]e^{ni\varphi}\}$$

$$+ R_o(\text{AC terms}) . \qquad \text{(A. 17)}$$

Since each Fourier coefficient in (A. 16) and (A. 17) must vanish,

$$\psi_{o,yyy} = -f_o + R_o\left[\tfrac{1}{2}\sum_{n=1}^{\infty} \mathrm{Im}(n\psi_n\bar{\psi}_{n,y})_{,y}\right] , \qquad \text{(A. 18)}$$

$$p_{o,y} = g_o - R_o\left[\tfrac{1}{2}\sum_{n=1}^{\infty} (n^2\psi_n\bar{\psi}_n)_{,y}\right] , \qquad \text{(A. 19)}$$

$$p_n = \frac{1}{ni}\left[f_n + \psi_{n,yyy} - n^2\psi_{n,y}\right] + 0(R_o), \quad n > 0, \text{ and} \qquad \text{(A. 20)}$$

$$p_{n,y} = g_n - ni\psi_{n,yy} + n^3 i\psi_n + 0(R_o) , \quad n > 0 . \qquad \text{(A. 21)}$$

Equations (A. 18), (A. 19), and (A. 20) correspond to (3. 9), (3. 10), and (3. 12) respectively. Equation (3. 11) is obtained from (A. 21) by elimination of $p_{n,y}$ using (A. 20).

Appendix B

Derivation of solution to (3. 11) subject to (3. 13), (3. 14), and (3. 15).

To order R_o equation (3. 11) may be written as

$$(D^2 - n^2)^2 \psi_n = \pi_n, \quad \text{where } D \equiv \frac{d}{dy}, \tag{B. 1}$$

or upon factoring the operator, we have

$$(D - n)^2 (D + n)^2 \psi_n = \pi_n. \tag{B. 2}$$

If we let $\Phi \equiv (D + n)^2 \psi_n$, then (B. 2) may be written as

$$\Phi_{,yy} - 2n \Phi_{,y} + n^2 \Phi = \pi_n. \tag{B. 3}$$

The solution to this second order, linear, inhomogeneous equation may be written down as

$$\Phi \equiv (D+n)^2\psi_n = (A_n y + B_n)e^{ny} + \int_o^y (y-y_1)e^{n(y-y_1)}\pi_n(y_1)dy_1, \tag{B. 4}$$

where A_n and B_n are arbitrary constants. Similarly, upon replacing n with -n we have

$$(D-n)^2\psi_n = (C_n y + D_n)e^{-ny} + \int_o^y (y-y_1)e^{-n(y-y_1)}\pi_n(y_1)dy_1, \tag{B. 5}$$

where C_n and D_n are arbitrary constants. Subtracting (B. 5) from (B. 4) we obtain

$$4n\psi_{n,y} = (A_n y + B_n)e^{ny} - (C_n y + D_n)e^{-ny} + \int_o^y (y-y_1)[e^{n(y-y_1)} - e^{-n(y-y_1)}]\pi_n(y_1)dy_1. \tag{B. 6}$$

Similarly, adding (B. 4) and (B. 5) we have

$$2(\psi_{n,yy} + n^2\psi_n) = (A_n y + B_n)e^{ny} + (C_n y + D_n)e^{-ny} + \int_o^y (y-y_1)[e^{n(y-y_1)} + e^{-n(y-y_1)}]\pi_n(y_1)dy_1 \tag{B. 7}$$

Elimination of $\psi_{n,yy}$ from (B. 7) using (B. 6) yields the general solution to (B. 1) which may be written as

$$\psi_n = \frac{1}{4n^2}\{[[A_n(y-\frac{1}{n})+B_n]+\int_o^y (y-y_1-\frac{1}{n})e^{-ny_1}\pi_n(y_1)dy_1]e^{ny} + [[C_n(y+\frac{1}{n})+D_n]+\int_o^y (y-y_1+\frac{1}{n})e^{ny_1}\pi_n(y_1)dy_1]e^{-ny}\}, \quad n>0. \tag{B. 8}$$

The constants A_n, B_n, C_n, and D_n are now determined by imposing the boundary conditions (3. 13) and (3. 14):

$$\psi_{n,y}(0) = 0 \Rightarrow D_n = B_n, \tag{B. 9}$$

$$\psi_n(0) = 0 \Rightarrow C_n = A_n - 2nB_n, \tag{B. 10}$$

$$\psi_n(\infty) = 0 \Rightarrow A_n = -\int_o^{kL} e^{-ny_1}\pi_n(y_1)dy_1, \tag{B. 11}$$

$$B_n = \int_o^{kL} y_1 e^{-ny_1}\pi_n(y_1)dy_1. \tag{B. 12}$$

Note that as a result of (3. 15), π_n vanishes identically for $y > kL$, so that the upper limits of integration in (B. 11) and (B. 12) need only be kL. Also from (B. 6) it is seen that (B. 11) and (B. 12) are compatible with the condition $\psi_{n,y}(\infty) = 0$. Upon substituting (B. 9) - (B. 12) into (B. 8), we obtain that to order R_o,

$$\psi_n = \frac{1}{4n^2} \{[\int_{kL}^{y} (y-y_1 - \frac{1}{n})e^{-ny_1} \pi_n(y_1)dy_1]e^{ny}$$

$$+ [\int_{o}^{y} (y-y_1 + \frac{1}{n})e^{ny_1} \pi_n(y_1)dy_1 - \int_{o}^{kL}(y+y_1+2nyy_1+\frac{1}{n})e^{-ny_1}$$

$$\pi_n(y_1)dy_1]e^{-ny}\} . \qquad \text{(B. 13)}$$

REFERENCES

Baba, S. A. and Hiramoto, Y. (1970). A quantitative analysis of ciliary movement by means of high-speed microcinematography. J. Exp. Biol. 52, 675-690.

Blake, J. R. (1971a). A spherical envelope approach to ciliary propulsion. J. Fluid Mech. 46, 199-208.

Blake, J. R. (1971b). Infinite models for ciliary propulsion. J. Fluid Mech. 49, 209-22.

Blake, J. R. (1971c). Self-propulsion due to oscillations on the surface of a cylinder at low Reynolds number. Bull. Aust. Math. Soc. 5, 255-64.

Blake, J. R. (1972). A model for the micro-structure in ciliated organisms. J. Fluid Mech. 55, 1-23.

Blake, J. R. (1973). A finite model for ciliated micro-organisms. J. Biomech. 6, 133-40.

Blake, J. R. and Sleigh, M. A. (1974). Mechanics of ciliary locomotion. Biol. Rev. 49, 85-125.

Brennen, C. (1974). An oscillating boundary layer theory for ciliary propulsion. J. Fluid Mech. 65, 799-824.

Bullington, W. E. (1930). A further study of spiraling in the ciliate Paramecium, with a note on morphology and taxonomy. J. Exp. Zoo. 56, 423-448.

Cheung, A. T. W. (1973). Determination of ciliary beat in Opalina obtrigonoidea. Ph. D. dissertation, University of California, Los Angeles.

Cheung, A. T. W. and Jahn, T. L. (1975). Helical nature of the continuous ciliary beat of Opalina. Acta Protozool. (in press).

Chwang, A. T. and Wu, T. Y. (1974). Hydromechanics of the low-Reynolds Number flows. Part 2. The singularity method for Stokes flows. J. Fluid Mech. 67, 787-815.

Cox, R. G. (1970). The motion of long slender bodies in a viscous fluid. Part 1. General theory. J. Fluid Mech. 44, 791-810.

Cox, R. G. (1971). The motion of long slender bodies in a viscous fluid. Part 2. Shear flow. J. Fluid Mech. 45, 625-657.

Gray, J. (1928). Ciliary Movement. Cambridge University Press.

Gray, J. and Hancock, G. J. (1955). The propulsion of sea-urchin spermatozoa, J. exp. Biol. 32, 802-14.

Hiramoto, Y. (1974). Mechanics of ciliary movement. In Cilia and Flagella (ed. M. A. Sleigh), pp. 177-196, Academic Press.

Katz, D. F. and Blake, J. R. (1974). Flagellar motions near a wall. In Proceedings of the Symposium on Swimming and Flying in Nature (in press).

Knight-Jones, E. W. (1954). Relations between metachronism and the direction of ciliary beat in Metazoa. Q. J. microsc. Sci. 95, 503-21.

Lighthill, M. J. (1952). On the squirming motion of nearly spherical deformable bodies through liquids at very small Reynolds numbers. Comm. Pure Appl. Math 5, 109-18.

Machemer, H. (1972a). Temperature influences on ciliary beat and metachronal coordination in Paramecium. J. Mechanochem. Cell Motility 1, 57-66.

Machemer, H. (1972b). Ciliary activity and origin of metachrony in Paramecium: Effects of increased viscosity. J. exp. Biol. 57, 239-59.

Naitoh, Y. (1958). Direct current stimulation of Opalina with intracellular micro-electrode. Ann. Zool. Jap. 31, 59-73.

Okajima, A. (1953). Studies on the metachronal wave in Opalina. I. Electrical stimulation with the micro-electrode. Jap. J. Zool. 11, 87-100.

Parducz, B. (1967). Ciliary movements and coordination in ciliates. Int. Rev. Cytol. 21, 91-128.

Satir, P. (1974). How cilia move. Sci. Am. 231, 44-52.

Sedar, A. W. and Porter, K. R. (1955). The fine structure of cortical components of Paramecium multimicronucleatum. J. biophys. Cytol. 1, 583-604.

Sleigh, M. A. (1960). The form of beat in cilia of Stentor and Opalina. J. exp Biol. 37, 1-10.

Sleigh, M. A. (1962). The biology of cilia and flagella. London: Pergamon.

Sleigh, M. A. (1968). Patterns of ciliary beating. Symp. Soc. exp. Biol. 22, 131-50.

Sleigh, M. A. (1969). Coordination of the rhythm of beat in some ciliary systems. Int. Rev. Cytol. 25, 31-54.

Sleigh, M. A. and Aiello, E. (1972). The movement of water by cilia. Acta Protozool. 11, 265-77.

Sleigh, M. A. and Holwill, M. E. J. (1969). Energetics of ciliary movement in Sabellaria and Mytilus. J. exp. Biol. 50, 733-43.

Tamm, S. L. and Horridge, G. A. (1970). The relation between the orientation of the central fibrils and the direction of beat of Opalina. Proc. R. Soc. Lond. B 175, 219-33.

Taylor, G. I. (1951). Analysis of swimming of microscopic organisms. Proc. R. Soc. Lond. A 209, 447-61.

Ueda, K. (1956). Intracellular calcium and cilia reversal in Opalina. Jap. J. Zool. 12, 1-10.

Winet, H. (1973). Wall drag on free-moving ciliated micro-organisms, J. exp. Biol. 59, 753-766.

Wu, T. Y. (1973). Fluid mechanics of ciliary propulsion. Proceedings of the Tenth Anniversary Meeting of the Society of Engineering Science. Publisher: Society of Engineering Science, Raleigh, North Carolina (in press).

PART II

A POROUS PROLATE SPHEROIDAL MODEL FOR CILIATED MICRO-ORGANISMS

1. Introduction

The manner in which various micro-organisms propel themselves, while captivating micro-biologists for centuries, has only recently attracted the attention of hydrodynamicists. Although micro-organisms are capable of moving in many fascinating ways, there are two predominant types of locomotion which taxonomists have long used as a basis for classification. Flagellates consist of a head and one or more long slender motile organelles called flagella. In almost all cases they move by propagating a wave or bend along their flagellum in a direction opposite to that of the overall mean motion. Ciliates, on the other hand, consist of a body that is covered by a great number of hair-like organelles called cilia. They move as a result of the concerted action produced by the beating of each individual cilium.

Since micro-organisms are minute in size, the Reynolds number based upon a certain characteristic dimension of the body ℓ and the speed of propulsion U is very small, i.e. $R_e = U\ell/\nu \ll 1$, ν being the kinematic viscosity coefficient of the liquid medium. For the motion of most protozoa, the Reynolds number is of the order of 10^{-2} or less. Hence the predominant forces acting on micro-organisms are viscous forces, the inertia forces being negligible. This fact prompted Taylor (1951) to pose the following question:

> "How can a body propel itself when the inertia forces, which are the essential element in self-propuslion of all large living or mechanical bodies, are small compared with the forces due to viscosity?"

In attempting to answer Taylor's question, most fluid mechanical research on cell motility so far has been on flagellated micro-organisms. This is probably because they are the easier system to model theoretically. The inert head creates a drag while the beating flagellum provides a thrust, and the condition that the thrust balance the drag yields a relationship between the speed of propulsion and the other fluid dynamical parameters of the motion. On the other hand, as the thrust and drag are inseparable for the momentum consideration of a ciliated micro-organism, hydrodynamical models proposed for dealing with the phenomena are necessarily more complex than those for flagellates. In contrast to the fluid mechanical research, however, most biological research on protozoa, in which motility is often used as an assay of internal cell functions, has been devoted to the ciliates. This is principally because, in comparison to the flagellates, they are easier to obtain and maintain in the laboratory.

Primarily due to the great complexity of ciliary movement, the existing theoretical models proposed for predicting the motion of ciliates have been noted to contain considerable shortcomings in adequately representing the physical phenomena. Several authors, including Blake (1971b, 1972), Brennen (1974), and Keller, Wu, and Brennen (1975) have considered geometrically simplified models involving planar or cylindrical surfaces of infinite extent. These infinite models have made important contributions to our understanding of several aspects of the problem. However, while these models can be used as local approximations where the ratio of the cilium length

to the radius of curvature of the cell surface is small, they are limited in their capacity to assess the effect of the finite three-dimensional shape of the organism upon its locomotion.

There have also been several theoretical investigations of ciliary locomotion using a spherical geometry. Lighthill (1952), Blake (1971a) and Brennen (1974) have considered the propulsion of spherically shaped micro-organisms using an envelope model based upon replacing the organism by a material envelope undergoing small amplitude undulations about a spherical shape. In each of these investigations, the assumptions were made that the fluid adheres to a material envelope covering the cilia (the no-slip condition) and that the envelope propagates small amplitude waves. While this approach has also illuminated certain important features of the phenomena, as pointed out by Blake and Sleigh (1974), the no-slip condition imposed on the flow at the envelope surface, and the small amplitude of the waves are assumptions not fully supported by physical observations.

To overcome these limitations, Blake (1973) considered a different approach to a finite model for a spherical ciliated micro-organism. In this approach two regions were considered: one being the cilia layer and the other the exterior flow field. The velocity field for the cilia layer was determined using an infinite flat plate model (cf. Blake, 1972), while the velocity field for the external region was taken to be the known solution for a translating sphere with both radial and azimuthal surface velocities (cf. Blake, 1971a). The two velocity fields were then matched at a spherical control surface covering the cilia. Velocity profiles could then be extended from the cilia layer

into the exterior field and the propulsion velocity could be determined. While Blake's finite model sheds considerable light for spherically shaped organisms, its validity for the large number of non-spherical shapes found in nature is not entirely clear.

In order to assess the effect of geometrical shape upon the locomotion of a ciliated micro-organism, a theoretical analysis is carried out in the present investigation to consider a prolate spheroidal shaped body of arbitrary eccentricity. The central concept of the model is to represent the micro-organism by a porous prolate spheroidal control surface upon which certain boundary conditions are prescribed on the tangential and normal fluid velocities. The principal advantage of this approach is that it allows the overall effect of the cilia to be represented by prescribed boundary conditions on a simple geometrical surface. Furthermore, since it has been shown that the oscillatory velocities created by the cilia decay rapidly with distance from the cell wall (Brennen, 1974; Keller, et. al., 1975), only the mean fluid velocities need be considered.

The development of the model proceeds in a manner aimed at understanding the mechanism of propulsion and the effect of the shape of the body on its locomotion. The geometry and boundary conditions are set forth explicitly in Section 2. As the viscous forces are predominant in comparison with the inertial forces at the low Reynolds numbers characteristic of micro-organism movement, the hydrodynamic equations of motion may be approximated by Stokes equations. In Section 3 these equations are solved subject to the appropriate boundary conditions. In Section 4 the condition that the total force

acting on a freely swimming organism must vanish then yields a relationship between the speed of propulsion, the parameters that characterize the boundary conditions, and the shape of the organism. Using this relationship in Section 5, we consider the energy expenditure by a ciliated micro-organism. These considerations lead in Section 6 to an estimate of the effect of shape upon the power required for the motility of a ciliate. In order to visualize the flow, an expression is obtained in Section 7 for the stream function of the flow field and the streamlines are determined and discussed for several cases. Finally, in Section 8 several experimental streak photographs of small neutrally bouyant spheres suspended in the fluid around actual micro-organisms are presented. In order to exhibit the drastic difference between the case of a self-propelling micro-organism and that of a dead specimen sedimenting under gravity, streak photographs have been obtained for both types of flow and are compared with their respective theoretically predicted streamlines.

2. Geometry and boundary conditions

Although ciliates have a wide variety of body shapes, a great number of them are approximately axisymmetric and can be suitably represented by a prolate spheroid. Some common examples include Tetrahymena pyriformis, Spirostomum ambiguum, and Paramecium multimicronucleatum (see figure 1). The equation describing the prolate spheroidal control surface S which represents the organism is

$$\frac{z^2}{a^2} + \frac{\rho^2}{b^2} = 1 \qquad (\rho^2 = x^2 + y^2, \quad a \geqslant b), \tag{1}$$

where a is the semi-major axis and b is the semi-minor axis. The focal length 2c and eccentricity e are related by

$$c = (a^2 - b^2)^{\frac{1}{2}} = ea \qquad (0 \leqslant e < 1). \tag{2}$$

The organism is assumed to be translating with respect to the laboratory frame with velocity $\underline{U} = U\underline{e}_z$ where $U > 0$, and $\underline{e}_z$ is a unit vector pointing in the plus z direction. The velocity field with respect to the laboratory frame will be denoted by $\underline{u}^{\ell}$. The velocity field $\underline{u}$ with respect to a coordinate system, fixed with respect to the organism (the body frame), with origin coinciding with and axes parallel to the laboratory frame is related to $\underline{u}^{\ell}$ by

$$\underline{u}^{\ell} = \underline{u} + \underline{U} \ . \tag{3}$$

In this formulation of the problem, the effect of the cilia on the fluid is represented by certain prescribed boundary conditions on the radial component of velocity u_n and on the tangential component of

velocity u_s at the control surface S. Axisymmetry about the z axis is assumed. Guided by physical observation and mathematical hindsight, we consider the boundary conditions

$$\underline{u} = -U\underline{e}_z \qquad \text{as } |\underline{x}| \to \infty \tag{4}$$

$$u_n = \underline{u} \cdot \underline{n} = -V_n(\underline{n} \cdot \underline{e}_z) \qquad \text{on S} \tag{5}$$

$$u_s = \underline{u} \cdot \underline{s} = -V_s(\underline{s} \cdot \underline{e}_z) \qquad \text{on S} \tag{6}$$

where $\underline{x}$ is the position vector, the constants V_n and V_s are regarded as parameters of the problem, and $\underline{n}$ and $\underline{s}$ are unit outward normal and tangential vectors respectively with the sense of $\underline{s}$ indicated in figure 2. It is a simple matter to show that $\underline{n}$ and $\underline{s}$ are related to $\underline{e}_z$ and the unit radial vector $\underline{e}_\rho$ by

$$\underline{n} = [(1 - e^2)^{\frac{1}{2}} z\underline{e}_z + (a^2 - z^2)^{\frac{1}{2}} \underline{e}_\rho] (a^2 - e^2z^2)^{-\frac{1}{2}}, \tag{7}$$

$$\underline{s} = [-(a^2 - z^2)^{\frac{1}{2}} \underline{e}_z + (1 - e^2)^{\frac{1}{2}} z\underline{e}_\rho] (a^2 - e^2z^2)^{-\frac{1}{2}}. \tag{8}$$

Physically, for $V_n > 0$ and $V_s > 0$, the situation described by (5) and (6) is one in which the lateral cilia impart a tangential slip velocity while fluid is sucked into the cilia layer on the anterior and expelled on the posterior side of the organism. The net flux of fluid into the cilia layer is zero as it must be by continuity.

These boundary conditions are, of course, far too simple to model accurately the flow produced by any real organism. This possible over-simplification notwithstanding, they were chosen so that

a relatively simple solution can be obtained to illustrate the basic mechanism of self-propulsion. We note that at any point on S, $\underline{n} \cdot \underline{e}_z = \cos\theta$ and $\underline{s} \cdot \underline{e}_z = -\sin\theta$, where θ is the angle subtended by $\underline{n}$ and $\underline{e}_z$. In this sense, (5) and (6) might be viewed as the leading terms in a Fourier expansion in θ of a more general boundary condition.

3. Solution

The basic equations to be solved are the Stokes equations:

$$\nabla p = \mu \nabla^2 \underline{u}, \tag{9}$$

$$\nabla \cdot \underline{u} = 0, \tag{10}$$

where p is the pressure and μ the coefficient of viscosity which is taken to be constant. The solution technique employed follows closely the singularity method for Stokes flows lucidly described by Chwang and Wu (1975). We construct the solution by employing a line distribution of Stokeslets and potential doublets between the two foci $z = -c$ and c in the form

$$\underline{u} = -U\underline{e}_z - \int_{-c}^{c} [\alpha \underline{U}_S(\underline{x} - \underline{\xi}; \underline{e}_z) - (c^2 - \xi^2)\beta \underline{U}_D(\underline{x} - \underline{\xi}; \underline{e}_z)]d\xi, \tag{11}$$

$$p = -\int_{-c}^{c} \alpha P_s(\underline{x} - \underline{\xi}; \underline{e}_z)d\xi, \tag{12}$$

where α and β are constants to be determined, $\underline{\xi} = \xi \underline{e}_z$, and

$$\underline{U}_s(\underline{x} - \underline{\xi}; \underline{e}_z) = \frac{\underline{e}_z}{R} + \frac{(\underline{e}_z \cdot \underline{R})\underline{R}}{R^3} \quad (\underline{R} = \underline{x} - \underline{\xi}, \quad R = |\underline{R}|), \tag{13}$$

$$P_s(\underline{x} - \underline{\xi}; \underline{e}_z) = 2\mu \frac{\underline{e}_z \cdot \underline{R}}{R^3}, \tag{14}$$

$$\underline{U}_D(\underline{x} - \underline{\xi}; \underline{e}_z) = \frac{-\underline{e}_z}{R^3} + \frac{3(\underline{e}_z \cdot \underline{R})\underline{R}}{R^5}. \tag{15}$$

The expressions (13) and (14) are the velocity and pressure of a Stokeslet, the fundamental solution to Stokes equations associated with a singular point force acting on the fluid given by

$$\underline{f}_s = 8\pi\mu\, \underline{e}_z\, \delta(\underline{x} - \underline{\xi}), \tag{16}$$

where $\delta(\underline{x} - \underline{\xi})$ is the three-dimensional Dirac delta function. In equation (15), $\underline{U}_D$ represents the velocity field of a potential doublet, which is also a solution of Stokes equations and is related to the Stokeslet by $\underline{U}_D = \nabla^2 \underline{U}_s$. Alternatively, $\underline{U}_D$ may be derived from a velocity potential

$$\phi_D = \frac{-\underline{e}_z \cdot \underline{R}}{R^3} . \tag{17}$$

The pressure associated with a potential doublet is zero, in accordance with the present low-Reynolds-number approximation. Equations (11) and (12) represent a linear superposition of the fundamental solutions. By virtue of their construction and the linearity of the problem, they satisfy Stokes equations (9) and (10) as well as the boundary condition (4) on $\underline{u}$ at infinity. The pressure may be gauged, of course, by the addition of an arbitrary constant. The integrated form of (11) and (12) may be written as

$$\begin{aligned} \underline{u} = \{ &- U - 2(\alpha + \beta) \log \frac{R_2 - (z-c)}{R_1 - (z+c)} \\ &+ \alpha\left(\frac{z+c}{R_1} - \frac{z-c}{R_2}\right) + 2\beta c\left(\frac{1}{R_1} + \frac{1}{R_2}\right)\} \underline{e}_z + \\ &\{(\alpha+2\beta)\rho\left(\frac{1}{R_1} - \frac{1}{R_2}\right) + \frac{2\beta z}{\rho}\left(\frac{z+c}{R_1} - \frac{z-c}{R_2}\right)\} \underline{e}_\rho , \end{aligned} \tag{18}$$

$$p = 2\mu a\left(\frac{1}{R_1} - \frac{1}{R_2}\right), \tag{19}$$

where

$$R_1 = [(z+c)^2 + \rho^2]^{\frac{1}{2}}, \qquad R_2 = [(z-c)^2 + \rho^2]^{\frac{1}{2}}. \tag{20}$$

To satisfy the boundary conditions (5) and (6), we note that on the control surface S

$$\rho^2 = (1-e^2)(a^2-z^2), \qquad R_1 = a+ez, \qquad R_2 = a-ez, \tag{21}$$

$$\log \frac{R_2 - (z-c)}{R_1 - (z+c)} = \log \frac{1+e}{1-e} \equiv L, \qquad (-a \leqslant z \leqslant a). \tag{22}$$

Consequently equation (18), when evaluated on the surface S, after some manipulation, gives for the surface velocity the result

$$\underline{u}_o = \left[-U-2aL+\beta\left(\frac{4e}{1-e^2}-2L\right)\right](\underline{n}\cdot\underline{e}_z)\underline{n} + \left[-U+2a(e-L)+2\beta(2e-L)\right](\underline{s}\cdot\underline{e}_z)\underline{s}, \tag{23}$$

where $\underline{n}$ and $\underline{s}$ are given by (7) and (8). Thus we find that (5) and (6) will be satisfied if

$$a = \frac{e^2}{(1+e^2)L-2e}\left[\frac{1}{1-\kappa}V_n + \frac{1}{1-\frac{1}{\kappa}}V_s - U\right], \tag{24}$$

$$\beta = \frac{1-e^2}{4e^3}\left[V_s - V_n + 2ea\right], \tag{25}$$

where

$$\kappa = \frac{2e-(1-e^2)L}{(1-e^2)(2e-L)} \quad . \tag{26}$$

It is noted that for $V_n = V_s = 0$, equations (24) and (25) reduce to the results of Chwang and Wu (1975) with U replaced by $-U_1$ for a rigid (no-slip) prolate spheroid translating parallel to its major axis. The above solution may also be derived from the Stokes stream function equation written in prolate spheroidal coordinates (see Happel and Brenner, 1973).

The drag experienced by the organism $\underline{D}$ comes only from the Stokeslets in the solution and may be evaluated simply by superposition to give

$$\underline{D} = -8\pi\mu \int_{-c}^{c} (-a\underline{e}_z)\, dz = 16\pi\mu c a \underline{e}_z. \tag{27}$$

In the limiting case of a sphere ($e \to 0$), (27) becomes

$$\underline{D} = -6\pi\mu a \left[\frac{1}{3}(U-V_n) - \frac{2}{3}(V_s - U)\right] \underline{e}_z, \tag{28}$$

while in the limiting case of a needle ($e \to 1$), (27) reduces to

$$\underline{D} = \frac{4\pi\mu a(V_s - U)}{\log\left(\frac{2a}{b}\right) - \frac{1}{2}} \underline{e}_z \quad . \tag{29}$$

Equations (28) and (29) reduce to well known results for translating rigid (no-slip) bodies when $V_s = V_n = 0$.

4. Self-propulsion

For a freely swimming organism, the total force acting on the body must be zero. From equations (27) and (24) we see that, in the absence of external forces, this condition will be satisfied if

$$U = \frac{1}{1-\kappa} V_n + \frac{1}{1-\frac{1}{\kappa}} V_s , \qquad (30)$$

where κ is given by (26). As e varies from 0 to 1, κ varies from -2 to $-\infty$. Thus it is seen that both the normal and tangential components contribute to the propulsion. If $V_s = 0$, the organism could still propel itself by the mechanism of suction and expulsion of fluid across the envelope of the cilia. If $V_n = 0$, the organism could propel itself through the mechanism of creating a slip velocity at the envelope.

The relationship between V_n/U and V_s/U for self-propulsion is indicated graphically in figure 3. The curves are a series of straight lines passing through the point ($V_n/U = 1$, $V_s/U = 1$) with slopes which depend on the eccentricity e and which have the limiting value of -2 for $e = 0$ and $-\infty$ for $e = 1$. The point ($V_n/U = 1$, $V_s/U = 1$) corresponds to the situation in which the organism has made itself "invisible" to the fluid. Indeed for this case $\alpha = \beta = 0$ (see (24) and (25)), and a trivial solution results. It is seen in general for a given speed of propulsion U, that as the slip velocity V_s increases, the necessary normal velocity V_n for zero drag decreases, and that this effect is enhanced as e goes to 1. Indeed, for V_s/U greater than 1.5, V_n/U must be negative. Physically this means that when V_s/U is large enough the surface integral of the wall shearing

stress in the plus z direction is so great, that for equilibrium it is necessary to have the contribution from the normal stress oppose the motion.

It is of interest to investigate the effect of the shape of the organism on its speed of propulsion. In the sphere limit ($e \to 0$), equation (30) becomes

$$U = \frac{1}{3} V_n + \frac{2}{3} V_s , \tag{31}$$

which is in agreement with Blake (1973) with V_s replaced by B_1 and V_n by $-A_1$, while in the needle limit ($e \to 1$) this condition becomes

$$U = V_s . \tag{32}$$

Plots of U/V_s verses e are drawn in figure 4 for various values of V_n/V_s. It is seen that for $V_n/V_s > 1$, U/V_s decreases with increasing eccentricity, whereas the opposite trend holds for $V_n/V_s < 1$. For most organisms the beat pattern of the cilia is conducive to creating tangential rather than normal velocities, so that we might expect $0 < V_n/V_s < 1$. In this range it may be observed that the speed of propulsion is not altered very much by the shape of the organism. This effect might partially explain why such a wide variety of shapes of ciliated creatures occur in nature.

From equations (11), (25), and (30) we find that the velocity field for a freely swimming organism ($a = 0$) is given by

$$(\underline{u})_{a=0} = -U\underline{e}_z + \beta_o \int_{-c}^{c} (c^2 - \xi^2) \underline{U}_D (\underline{x} - \underline{\xi}; \underline{e}_z) d\xi , \tag{33}$$

where

$$\beta_o = \frac{(1-e^2)(U-V_n)}{2[2e-(1-e^2)L]} . \tag{34}$$

It is of interest to note from the work of Chwang and Wu (1974), that the velocity field for the potential flow created by a uniform axial flow $-U\underline{e}_z$ past a prolate spheroid, of eccentricity e' and focal length c, may be represented by

$$\underline{u}' = -U\underline{e}_z + \beta' \int_{-c}^{c} (c^2 - \xi^2)\, \underline{U}_D(\underline{x} - \underline{\xi}; \underline{e}_z)d\xi , \tag{35}$$

where

$$\beta' = \frac{(1-e'^2)U}{2[2e' - (1-e'^2)L']} \tag{36}$$

with $L' = \log [(1+e')/(1-e')]$. Upon comparison of (34) and (36) we see that the velocity field for a swimming prolate spheroidal shaped organism of focal length c and eccentricity e is equivalent to the potential flow past a prolate spheroid of the same focal length and eccentricity e' defined by the solution of the transcendental equation

$$\frac{(1-e'^2)}{[2e' -(1-e'^2)L']} = \frac{(1-e^2)}{[2e - (1-e^2)L]} \left(1 - \frac{V_n}{U}\right) . \tag{37}$$

Since the expression on the left hand side is a decreasing function of e', we see that for $0 < V_n/U < 1$, the equivalent potential flow prolate spheroid would be more slender.

5. Energy dissipation

As a ciliated micro-organism swims through a fluid, energy is being dissipated by viscosity in the fluid both inside and outside the cilia layer. While an estimate of the former is difficult, the present model allows an evaluation of the latter.

If we regard V as the volume exterior to the control surface S, then it is a well known result (see e. g. Lamb, 1932) that the rate at which energy is being dissipated by viscosity in the fluid occupying V is

$$\dot{E} = -\int_S (\sigma \underline{n}) \cdot \underline{u}^{\ell} \, dS \, , \tag{38}$$

where σ is the Newtonian stress tensor $-pI + \mu[(\nabla \underline{u}) + (\nabla \underline{u})^T]$, I being the unit tensor and T indicating the transpose, and $\underline{n}$ is the unit outward normal to S as before. By employing equation (3) we may write equation (38) as

$$\dot{E} = -\int_S (\sigma \underline{n}) \cdot \underline{u} \, dS - \underline{U} \int_S (\sigma \underline{n}) \, dS. \tag{39}$$

Since the second integral in (39) is just the drag experienced by the body, we may write

$$\dot{E} = -\int_S (\sigma \underline{n}) \cdot \underline{u} \, dS + \underline{F} \cdot \underline{U} \, , \tag{40}$$

where $\underline{F}$ is the external force equal and opposite to the drag that must be applied to the body in order to maintain such a fluid motion. This equation asserts that the rate at which energy is being dissipated by

viscosity is equal to the rate at which work is done by the surface forces at surface S plus the rate at which work is done by the external force $\underline{F}$. We note that for an impermeable rigid body, $\underline{u} = \underline{0}$ on S, and $\dot{E}$ reduces to $\underline{F} \cdot \underline{U}$. For example, in the fall of a solid sphere the rate of work done by gravity is $6\pi\mu a U^2$ which is the rate of energy dissipation by viscosity.

The evaluation of (38) for the present case is somewhat tedious and the details are given in the Appendix. The result is

$$\dot{E} = 8\pi\mu a[(1+e^2)L - 2e][\frac{3-e^2}{e}\alpha^2 - 4e\alpha\beta + \frac{4e^3}{1-e^2}\beta^2] , \qquad (41)$$

where α and β are given by (24) and (25) and $L = \log[(1+e)/(1-e)]$ as before. For a freely swimming organism ($\alpha = 0$) it is found from equations (25), (26), (30), and (41) that the rate of energy expenditure outside the cilia layer is given by

$$\dot{E}_o = \frac{8\pi\mu a[(1+e^2)L - 2e](1-e^2)e^3}{[2e - (1-e^2)L]^2}(U - V_n)^2 . \qquad (42)$$

For the case of an inert body ($V_n = V_s = 0$), by using (24), (25), and (41), it is seen that the power required would be

$$\dot{E}_I = \frac{16\pi\mu a e^3}{[(1+e^2)L - 2e]} U^2 . \qquad (43)$$

We see that this expression is in agreement with the expected result that $\dot{E}_I = -\underline{D} \cdot \underline{U}$ (cf. equations (24) and (27) with $V_n = V_s = 0$).

6. The effect of shape upon energy expenditure

A large number of shapes of ciliated micro-organisms occur in nature. For example Icthyophthirius multifilis and Balantidium coli are nearly spherical while Paramecium multimicronucleatum and Spirostomum ambiguum are very slender and elongated. In contrast most fish, while differing in size, have the same general geometrical shape. Furthermore, many individual micro-organisms can alter their shape; Spirostomum a. can tie itself into a knot.

In the light of the above, it is of interest to investigate the effect of the shape of our model organism, as measured by its eccentricity, upon the rate of energy expenditure. We note that $\dot{E}$ as given by (41) depends upon the length of the major semi-axis of the body, a; that is, (41) expresses the rate of energy expenditure for a body of constant length. Physically, however, it is more significant to consider the effect of shape upon a body of constant volume (i. e. mass). In this regard, we note that the volume V_o of a prolate spheroid is given by

$$V_o = \frac{4}{3}\pi a^3(1-e^2) \tag{44}$$

Therefore for a given V_o, the semi-major axis necessary to maintain a constant volume is

$$a = \frac{a_o}{(1-e^2)^{1/3}} \tag{45}$$

where $a_o = (3V_o/4\pi)^{1/3}$. Upon substituting (45) into (41), we obtain for the rate of energy expenditure at constant volume

$$(\dot{E})_{V_o} = \frac{8\pi\mu a_o[(1+e^2)L-2e]}{(1-e^2)^{1/3}}\left[\frac{3-e^2}{e}\alpha^2 - 4e\alpha\beta + \frac{4e^3}{1-e^2}\beta^2\right] . \tag{46}$$

Figure 5 is a plot of $(\dot{E})_{V_o}$, non-dimensionalized by $6\pi\mu a_o U^2$, versus the eccentricity for constant values of V_n/U. The center curve labelled $V_n/U = 0$, $V_s/U = 0$ corresponds to the translation of an inert impermeable body. Since there is a drag on the body, an external force would be needed to achieve the motion. As the body becomes slender, the drag per unit length diminishes logarithmically (cf. (29)), but the length necessary to maintain a constant volume grows algebraically (cf. (45)). Thus $(\dot{E})_{V_o}$ is fairly constant until it becomes singular for very high eccentricity.

The other curves correspond to the case of a freely swimming organism ($\alpha = 0$). The tangential velocity component, as previously shown, would vary with eccentricity in order to keep $\alpha = 0$ (cf. (30) or figure 3). For $V_n/U = 0$, 0.2, and 0.4 it is found that V_s/U varies from 1.5 to 1 , 1.4 to 1, and 1.3 to 1 respectively as e goes from 0 to 1. It is seen that for constant V_n/U, $(\dot{E})_{V_o}$ for a freely swimming organism decreases with eccentricity. Furthermore, for constant eccentricity, $(\dot{E})_{V_o}$ decreases for increasing V_n/U within the range $0 < V_n/U < 1$. It is of interest to note that for a sufficiently slender shape (or V_n/U large enough), $(\dot{E})_{V_o}$ is less than the power required to propel an inert impermeable body at the same speed.

In order to compare the energy expenditure within the cilia layer to that outside the cilia layer, we consider a specific organism,

Paramecium multimicronucleatum. Using simple resistive theory, several authors including Yoneda (1962), Sleigh and Holwill (1969), Hiramoto (1974), and Keller (1975) have estimated the local rate of working of a single cilium. It appears that a conservative estimate of the local rate of working of a single cilium of Paramecium m. within the cilia layer would be 1×10^{-7} ergs/sec. For a typical organism $a = 80\ \mu m$ and $b = 30\ \mu m$ (cf. figure 1), and the surface density of cilia is about 0.267 cilia/μm^2 (Sleigh, 1969). Therefore, if we assume that each cilium works at the same rate, the energy expenditure rate within the cilia layer is about 6.7×10^{-4} ergs/sec. The nominal swimming speed of Paramecium m. is observed to be about 2500 μm/sec. Assuming $V_n = 0$, we find from equation (42) that the energy expenditure rate outside the cilia layer, $\dot{E}_o$, is about 3.0×10^{-5} ergs/sec. Therefore we see that for a freely swimming organism most of the power required for motility is expended in the fluid within the cilia layer.

In summary, therefore, the slenderness of the body greatly diminishes the rate of energy spent in the fluid outside the cilia layer. However, since this is probably a small percentage of the energy expended in the fluid within the cilia layer, the efficiency of propulsion would not appear to be greatly altered by the shape of the organism. This conclusion again indicates that this mechanism of propulsion affords an evolutionary advantage.

7. The stream function

In order to visualize the flow field around a micro-organism, we consider the Stokes stream function ψ defined by the equations

$$-\frac{1}{\rho}\frac{\partial\psi}{\partial\rho} = u_z^{\ell} \quad , \tag{47}$$

$$\frac{1}{\rho}\frac{\partial\psi}{\partial z} = u_\rho^{\ell} \quad , \tag{48}$$

where $u_\rho^{\ell} = \underline{u}^{\ell} \cdot \underline{e}_\rho$ and $u_z^{\ell} = \underline{u}^{\ell} \cdot \underline{e}_z$. Making use of the integrated form of $\underline{u}$ from equation (18), we may write (47) and (48) as

$$\frac{\partial\psi}{\partial\rho} = -\rho\{-2(\alpha+\beta)\log\frac{R_2-(z-c)}{R_1-(z+c)} + \alpha\,(\frac{z+c}{R_1} - \frac{z-c}{R_2}) + 2\beta c(\frac{1}{R_1} + \frac{1}{R_2})\} \, , \tag{49}$$

$$\frac{\partial\psi}{\partial z} = \rho\{(\alpha+2\beta)\rho(\frac{1}{R_1} - \frac{1}{R_2}) + \frac{2\beta z}{\rho}(\frac{z+c}{R_1} - \frac{z-c}{R_2})\} \, , \tag{50}$$

where $R_1 = [(z+c)^2 + \rho^2]^{\frac{1}{2}}$ and $R_2 = [(z-c)^2 + \rho^2]^{\frac{1}{2}}$ as before. To integrate the first of these, we note that integration by parts yields the result

$$\int \rho \log\frac{R_2-(z-c)}{R_1-(z+c)}\, d\rho = \frac{\rho^2}{2}\log\frac{R_2-(z-c)}{R_1-(z+c)} + \frac{1}{2}[(z+c)R_1-(z-c)R_2] \, . \tag{51}$$

Thus, integration of equation (49) yields

$$\psi = (\alpha+\beta)\rho^2 \log \frac{R_2-(z-c)}{R_1-(z+c)} + \beta[(z-c)R_1-(z+c)R_2] + f(z), \tag{52}$$

where f is a function of z only. Similarly, integration of (50) yields

$$\psi = (\alpha+\beta)\rho^2 \log \frac{R_2-(z-c)}{R_1-(z+c)} + \beta[(z-c)R_1-(z+c)R_2] + g(\rho) \tag{53}$$

where g is a function of ρ only. Comparing (52) and (53) we see that

$$f(z) = g(\rho) = \psi_o \ , \tag{54}$$

where ψ_o is a constant. Without loss of generality we may take $\psi_o = 0$. Thus the stream function corresponding to the solution of the problem is

$$\psi = (\alpha+\beta)\rho^2 \log \frac{R_2-(z-c)}{R_1-(z+c)} + \beta[(z-c)R_1-(z+c)R_2] \ , \tag{55}$$

where α and β are given by (24) and (25). Once α and β have been determined by specifying U, V_n, V_s, and e (see (24) and (25)), the streamlines in any meridian plane may be found from (55).

In order to illustrate the difference in the streamlines in going from a translating inert impermeable body to a self-propelling organism, we consider the streamlines in the laboratory frame about a prolate spheroid of eccentricity equal to 0.9 for three different cases. In case I we consider a translating inert (no slip) body specified by $V_n/U = 0$ and $V_s/U = 0$. Equations (24) and (25) imply that α/U =

-0.229 and $\beta/U = -0.027$. Again in order to achieve such a flow, an external force must act on the body in order to compensate the drag which is given by equation (27). The streamlines, which are plotted in figure 6, are open in the sense that they terminate at infinity. They are similar to the pattern for a sphere (see e. g. Lamb, 1932).

In case II we consider an organism for which $V_n/U = 0$ and $V_s/U = 1.17$. Equations (24) and (25) now imply that $\alpha/U = -0.001$ and $\beta/U = 0.076$, so that such a body would experience a slight drag. The streamlines for this case are plotted in figure 7. Now some of the streamlines have two branches, one of which is closed.

Finally in case III we consider a freely swimming organism for which $\alpha/U = 0$ and thus $\underline{D} = \underline{0}$ (see equation 27). As β now becomes simply a multiplicative factor in (55), the streamlines have the same form for any set of U, V_n, V_s, and e satisfying (30). The streamlines shown in figure 8 are all closed except for the trivial one given by $\rho = 0$.

8. Streak photographs of the flow around Paramecium

Since the theoretical model developed in this investigation predicts a great difference in the appearance of the streamlines for an inert body and a freely swimming micro-organism, an attempt has been made to verify the model, at least qualitatively, by means of the visualization of the streamlines around actual micro-organisms.

For this purpose specimens of Paramecium caudatum were prepared in an aqueous medium in which neutrally bouyant spheres (of 1 μm diameter) were suspended to serve as tracers of the flow field. A Nikon microscope (model L-ke) was employed to achieve a magnification of 200 and the images were recorded on 35 mm film (Kodak 2475) using a Nikon camera (model F). The illumination was by a Strobe (Strobex No. 71B) flashing at 6-24 Hz., and the shutter was left open for 1/4-2 sec., allowing for about 2-48 multiple exposures.

Figure 9 is a typical streak photograph of a freely swimming Paramecium caudatum. The exposure time was 1/2 sec. and the Strobe frequency was 24 Hz. The streak paths of the tracer spheres around the micro-organism are seen to be at least qualitatively in agreement with figure 8.

Since Paramecium caudatum is slightly denser than water, it was also possible to visualize the streamlines around an inert body propelled by an external force (viz. gravity). This was accomplished by carefully killing the organisms (for which purpose gentle heat is recommended) and by mounting the microscope on its side so as to have the microscopic slide inclined to the horizontal. Figure 10 is a

typical streak photograph of a dead Paramecium caudatum falling under the influence of gravity. The exposure time was 1.5 sec. and the strobe frequency was 10 Hz. The organisms fell at about 1/10 their freely swimming speed. Again comparison of the particle paths with figure 6 indicates a qualitative agreement between theory and experiment.

In comparing the photographs with the theoretical streamlines, one should keep in mind that the theory did not take into account the effect of the walls and other flow boundaries that were present in the experiment. The specimen preparations were made using a glass slide and a standard vaseline mount in which the coverslip was supported by a certain thickness of vaseline around its perimeter. Although exact measurements were difficult to obtain, this thickness was many times the length of the organism, and care was taken to focus at the central plane of the preparation.

In this regard we note that the inert sedimenting specimens displayed the streamlines that closely resemble the Stokes flow in the near field as opposed to the potential flow streamlines past a freely swimming body of the same shape. At large distances (more than a few body lengths away) from the inert specimen, however, the streamlines are expected to be significantly modified by the wall effects for at least two reasons. First, since the Stokes flow generated by an external force has a velocity field of much longer range than the corresponding potential flow, we may expect it to be subject to relatively stronger wall corrections. Second, the flow may exhibit features relating to the Hele-Shaw effect. According to the Hele-Shaw effect, a body, whose

dimensions are large compared to the thickness between two flat plates, will produce the streamlines of a potential flow in the gap when the inertial forces are negligible (see e. g. Batchelor, 1967).

9. Concluding remarks

The concept of representing a freely swimming micro-organism by a porous prolate spheroid leads to a reasonably successful model for the mechanism of locomotion. The principal advantage of this approach is that it allows us to incorporate the effect of the cilia into prescribed boundary conditions on a simple geometrical control surface.

With the proposed boundary conditions, which seem to be physically reasonable and which are characterized by only two parameters, several features of the propulsion of a prolate-spheroidal ciliated creature may be ascertained. It is found that, within the typical range of parameter values, the speed of propulsion is fairly insensitive to the eccentricity of the body. Furthermore, while the rate at which energy is expended in the fluid outside the cilia layer diminishes with slenderness, this component is seen to be only a small percentage of the power expended within the cilia layer. Therefore the rate of total energy expenditure for propulsion may be expected to depend primarily on the configuration of ciliary movement within the cilia layer rather than on the body shape. These conclusions may partially explain the occurrence of a great variety of shapes for ciliated creatures, and may indicate that this manner of locomotion affords an evolutionary advantage.

Another feature predicted by the model is a vast difference in the streamlines for the translation of an inert impermeable body and a freely swimming micro-organism of the same shape. Qualitatively, good agreement is found between the theoretically predicted streamlines

and experimental streak photographs of freely swimming and inert sedimenting micro-organisms.

It is hoped that the present investigation will serve to lay the groundwork for further improvement of the model that will enhance its versatility and accuracy in application to the phenomena of ciliary propulsion. As an initial step in this regard, one might consider more generalized boundary conditions in order to facilitate a matching of the exterior flow field to any suitable model for the flow within the cilia layer. We note that recently in a separate approach, Brennen (1975) has considered a similar geometry in which an exterior flow field equivalent to the present solution was matched to an envelope model. While the results of this analysis are not without merit, in view of the limitations of the envelope model it would be of interest to consider a treatment in which the flow in the vicinity of the cilia layer were represented more accurately. Here the singularity methods for Stokes flows may play a significant role. A further improvement, which would be of practical value in the laboratory, would be to consider the effect of the proximity of the organism to walls.

Appendix. Evaluation of the rate of energy dissipation

In this appendix we evaluate equation (38) which may be written as

$$\dot{E} = \dot{E}_p + \dot{E}_\tau , \tag{56}$$

where

$$\dot{E}_p = \int_S (p\underline{n}) \cdot \underline{u}^{\ell} \, dS , \tag{57}$$

$$\dot{E}_\tau = -\int_S (\tau \underline{n}) \cdot \underline{u}^{\ell} \, dS , \tag{58}$$

where τ is the viscous stress tensor given by

$$\tau = \mu[(\nabla \underline{u}) + (\nabla \underline{u})^T] , \tag{59}$$

with T indicating the transpose. We note that an element of surface area of the prolate spheroid is given by

$$dS = 2\pi(1-e^2)^{\frac{1}{2}} (a^2 - e^2 z^2)^{\frac{1}{2}} \, dz, \qquad (-a \leqslant z \leqslant a) , \tag{60}$$

From equations (19) and (21) it is easily found that the pressure on surface S is given by

$$p_o = \frac{-4\mu a e z}{a^2 - e^2 z^2} , \qquad (-a \leqslant z \leqslant a) . \tag{61}$$

Employing equations (61), (60), (23), (7), and (3), we have for equation (57)

$$\dot{E}_p = -8\pi\mu a e(1-e^2)[-2aL + \beta(\frac{4e}{1-e^2} - 2L)] \int_{-a}^{a} \frac{z^2 dz}{a^2 - e^2 z^2} . \tag{62}$$

The integral may be readily evaluated to yield

$$\dot{E}_p = 16\pi\mu a \frac{(2e-L)}{e^2} \{-a^2(1-e^2) L + [2e-(1-e^2)L]\alpha\beta\} . \qquad (63)$$

To evaluate equation (58) it is convenient to express the velocity field in terms of prolate spheroidal coordinates (ξ, η, ϕ) defined by the transformation

$$z + i\rho = c \cosh(\xi + i\eta), \quad (0 < \xi < \infty, \ 0 < \eta < \pi, \ c > 0) . \qquad (64)$$

For convenience we define

$$\tau = \cosh \xi, \quad \zeta = \cos \eta \qquad (1 < \tau < \infty, \ -1 \leqslant \zeta \leqslant 1). \qquad (65)$$

From (64) and (65) it is found that

$$\rho = c\sqrt{\tau^2 - 1}\ \sqrt{1 - \zeta^2} \qquad \text{and} \qquad z = c\tau\zeta . \qquad (66)$$

The coordinate surface defined by τ = a constant is a prolate spheroid whose eccentricity is given by $e = 1/\tau$ with foci at $z = \pm$ c. The unit vector tangential to the τ coordinate curve is just $\underline{n}$, while the unit vector tangential to the ζ coordinate curve is $\underline{s}$. Thus we may write for the velocity field

$$\underline{u}^{\ell} = u_1(\tau, \zeta)\, \underline{n} + u_2(\tau, \zeta)\, \underline{s} . \qquad (67)$$

By substituting $c\tau\zeta$ for z and $1/\tau$ for e into equations (23), (8), and (7), we obtain after some manipulations

$$u_1 = \frac{2\zeta f}{\sqrt{\tau^2 - \zeta^2}\sqrt{\tau^2 - 1}} , \qquad (68)$$

$$u_2 = \frac{-\sqrt{1-\zeta^2}\ f'}{\sqrt{\tau^2-\zeta^2}}\ , \tag{69}$$

where

$$f = 2\beta\tau + (\alpha+\beta)(1-\tau^2)\log\ (\frac{\tau+1}{\tau-1}), \tag{70}$$

and a prime denotes differentiation with respect to τ. In prolate spheroidal coordinates the integrand of equation (58) may be expressed as (see e. g. Happel and Brenner, 1973)

$$\begin{aligned}\{[(\nabla\underline{u}) + (\nabla\underline{u})^T]\,\underline{n}\}\cdot\underline{u}^{\ell} = -2u_1 h[\frac{\partial u_1}{\partial q_1} + hu_2\ \frac{\partial}{\partial q_2}(\frac{1}{h})] \\ - u_2 h[\frac{\partial u_2}{\partial q_1} - hu_1\ \frac{\partial}{\partial q_2}(\frac{1}{h}) + \frac{\partial u_1}{\partial q_2} - hu_2\ \frac{\partial}{\partial q_1}(\frac{1}{h})]\ ,\end{aligned} \tag{71}$$

where $q_1 = \xi$, $q_2 = \eta$, and h is the metrical coefficient $1/c(\sinh^2\xi + \sin^2\eta)^{\frac{1}{2}}$. In terms of τ and ξ we note that

$$\frac{\partial}{\partial q_1} = \sqrt{\tau^2-1}\ \frac{\partial}{\partial\tau}\ , \qquad \frac{\partial}{\partial q_2} = -\sqrt{1-\zeta^2}\ \frac{\partial}{\partial\zeta}\ , \text{ and} \tag{72}$$

$$h = \frac{1}{c\sqrt{\tau^2-\zeta^2}}\ . \tag{73}$$

Furthermore, an element of surface area is given by (cf. Happel and Brennen)

$$dS = -2\pi c^2\sqrt{\tau^2-\zeta^2}\ \sqrt{\tau^2-1}\ d\zeta \qquad (-1 \leqslant \zeta \leqslant 1). \tag{74}$$

Equation (58) may now be evaluated by employing equations (68) - (74). This calculation is lengthy but straightforward and involves only some elementary integrals. Upon evaluating the result on the particular prolate spheroid $\tau = 1/e$, it is found, after considerable algebraic manipulation, that

$$\dot{E}_{\tau} = 8\pi\mu a \{\{2(e^2-3) + [(7-2e^2-e^4)e^{-1}]L + [-2(1-e^2)e^{-2}]L^2\}\alpha^2$$

$$+ \{-8(1-e^2) + [4(2-2e^2-e^4)e^{-1}]L + [-2(1-e^2)e^{-2}]L^2\}\alpha\beta$$

$$+ \{-8e^4(1-e^2)^{-1} + [4e^3(1+e^2)(1-e^2)^{-1}]L\}\beta^2. \tag{75}$$

The addition of equations (75) and (63) yields equation (41).

REFERENCES

Batchelor, G. K. 1967 An Introduction to Fluid Dynamics. Cambridge University Press.

Blake, J. R. 1971a A spherical envelope approach to ciliary propulsion. J. Fluid Mech. 46, 199-208.

Blake, J. R. 1971b Infinite models for ciliary propulsion. J. Fluid Mech. 49, 209-222.

Blake, J. R. 1972 A model for the micro-structure in ciliated organisms. J. Fluid Mech. 55, 1-23.

Blake, J. R. 1973 A finite model for ciliated micro-organisms. J. Biomech. 6, 133-140.

Blake, J. R. and Sleigh, M. A. 1974 Mechanics of ciliary locomotion. Biol. Rev. 49, 85-125.

Brennen, C. 1974 An oscillating-boundary-layer theory for ciliary propulsion. J. Fluid Mech. 65, 799-824.

Brennen, C. 1975 Hydromechanics of propulsion for ciliated microorganisms. Proceedings of the Symposium on Swimming and Flying in Nature (in press).

Chwang, A. T. and Wu, T. Y. 1974 A note of potential flow involving prolate spheroids. Schiffstech. 21, 19-31.

Chwang, A. T. and Wu, T. Y. 1975 Hydromechanics of low-Reynolds-number flow. Part 2. Singularity method for Stokes flows. J. Fluid Mech. 67, 781-815.

Happel, J. and Brenner, H. 1973 Low Reynolds Number Hydrodynamics. Nordoff.

Hiramoto, Y. 1974 Mechanics of ciliary movement. In Cilia and Flagella (ed. M. A. Sleigh). Academic Press.

Keller, S. R., Wu, T. Y., and Brennen, C. 1975 A traction-layer model for ciliary propulsion. Proceedings of the Symposium on Swimming and Flying in Nature (in press).

Lamb, H. 1932 Hydromechanics. Cambridge University Press.

Lighthill, M. J. 1952 On the squirming motion of nearly spherical deformable bodies through liquids at very small Reynolds numbers. Comm. Pure Appl. Math. 5, 109-118.

Sleigh, M. A. 1969 Coordination of the rhythm of beat in some ciliary systems. Int. Rev. Cytol. 25, 31-54.

Sleigh, M. A. and Holwill, M. E. J. 1969 Energetics of ciliary movement in Sabellaria and Mytilus. J. exp. Biol. 50, 733-743.

Taylor, G. I. 1951 Analysis of swimming of microscopic organisms. Proc. R. Soc. Lond. A 209, 447-61.

Yoneda, M. 1962 Force exerted by a single cilium of Mytilus Edulis. J. exp. Biol. 39, 307-317.

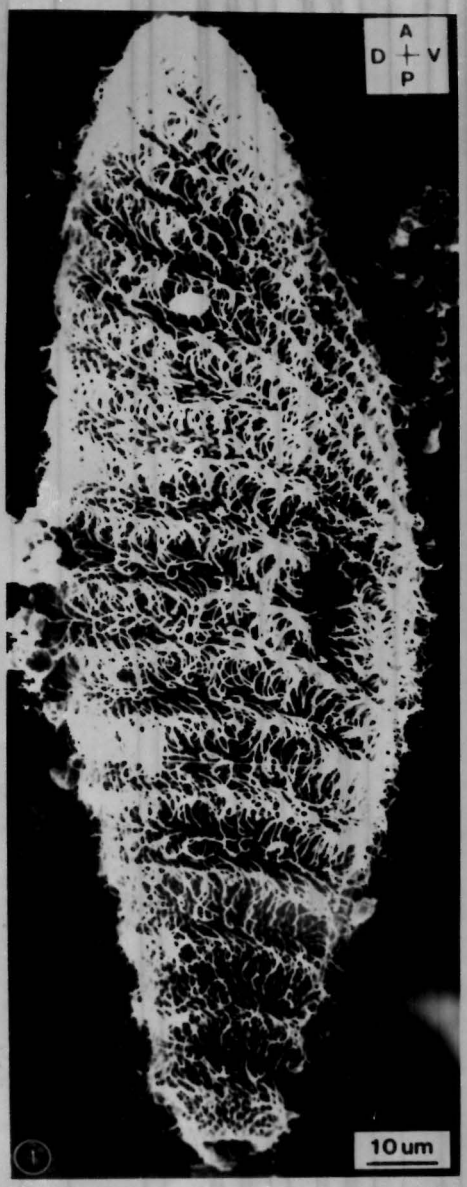

Figure 1. Scanning electron micrograph of Paramecium multimicronucleatum. (Courtesy S. L. Tamm)

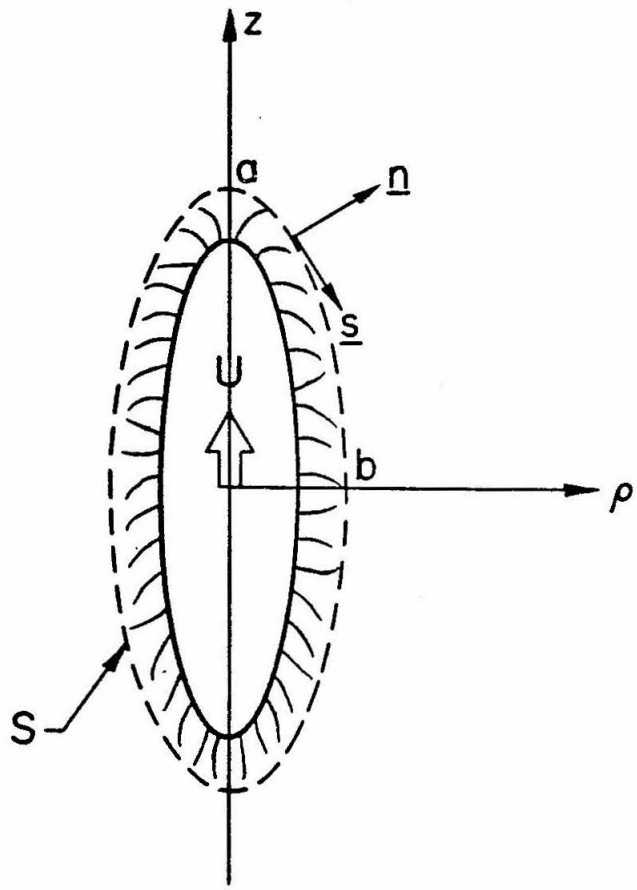

Figure 2. The geometry of the model in a meridian plane illustrating the body of the organism, the cilia layer, and the control surface S.

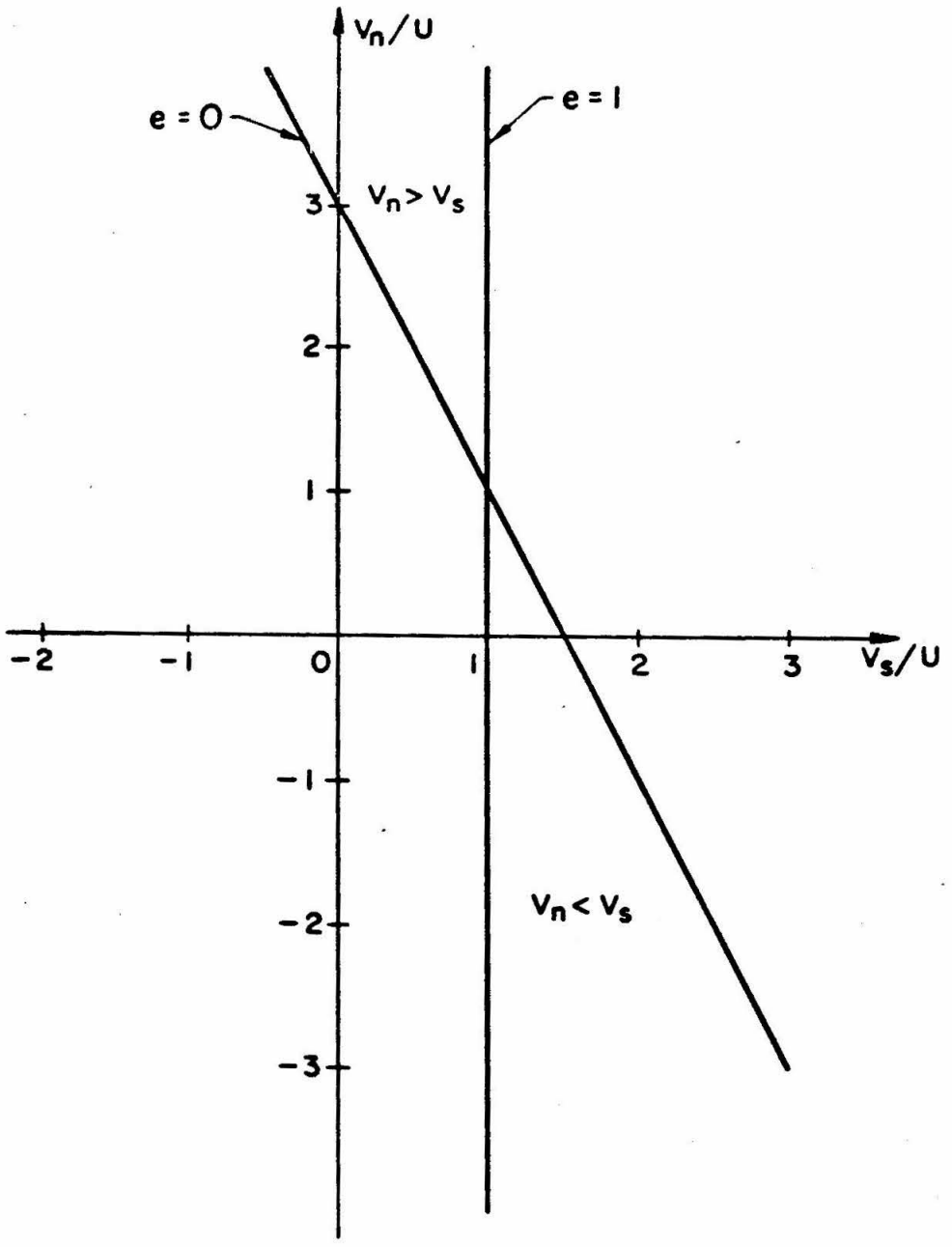

Figure 3. The relationship between V_n/U and V_s/U for self-propulsion.

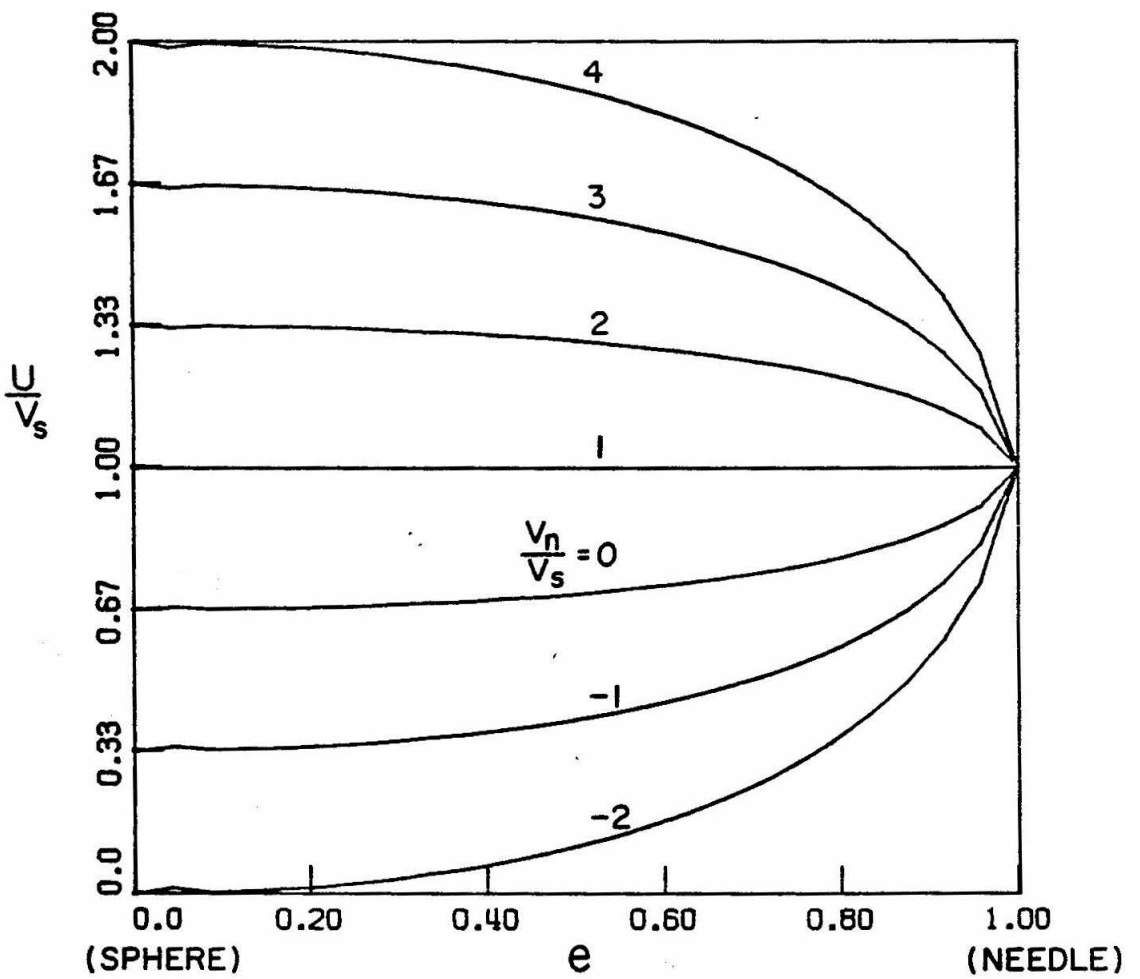

Figure 4. Variation of the speed of propulsion U with the eccentricity of the body e. The numbers indicate different values of V_n/V_s where V_n is the maximum suction velocity and V_s the maximum slip velocity created by the cilia.

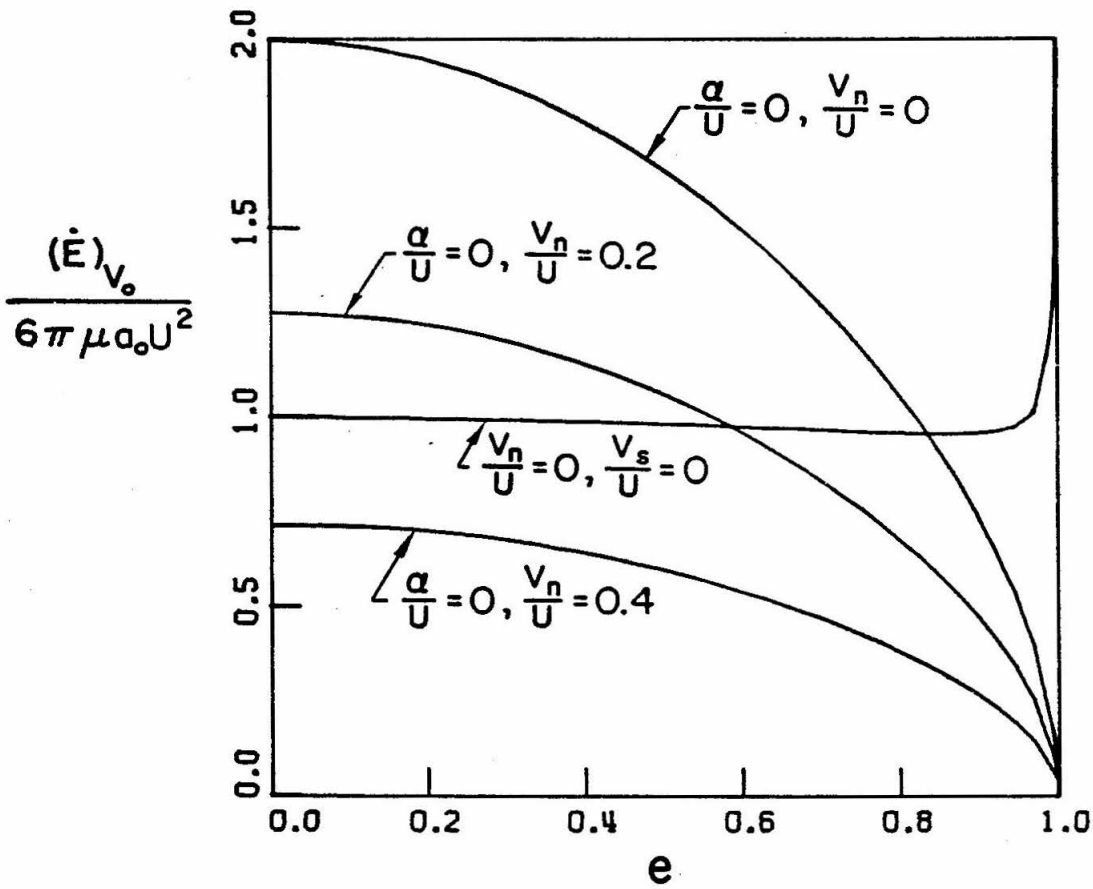

Figure 5. Variation of the rate of energy expenditure for a body of constant volume with eccentricity. The energy expenditure rate has been non-dimensionalized by $6\pi\mu a_o U^2$.

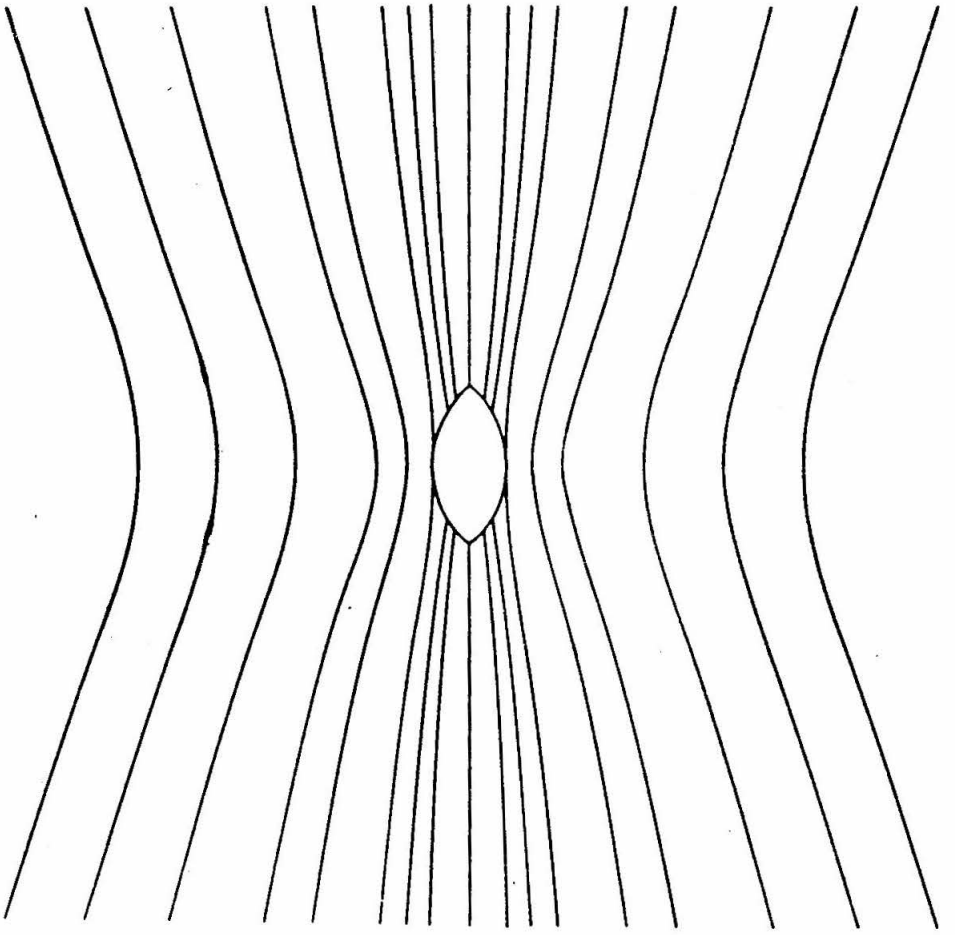

Figure 6. The streamlines ψ/c^2U in the laboratory frame for an inert translating prolate spheroid of eccentricity 0.9. Here $V_n/U = V_s/U = 0$.

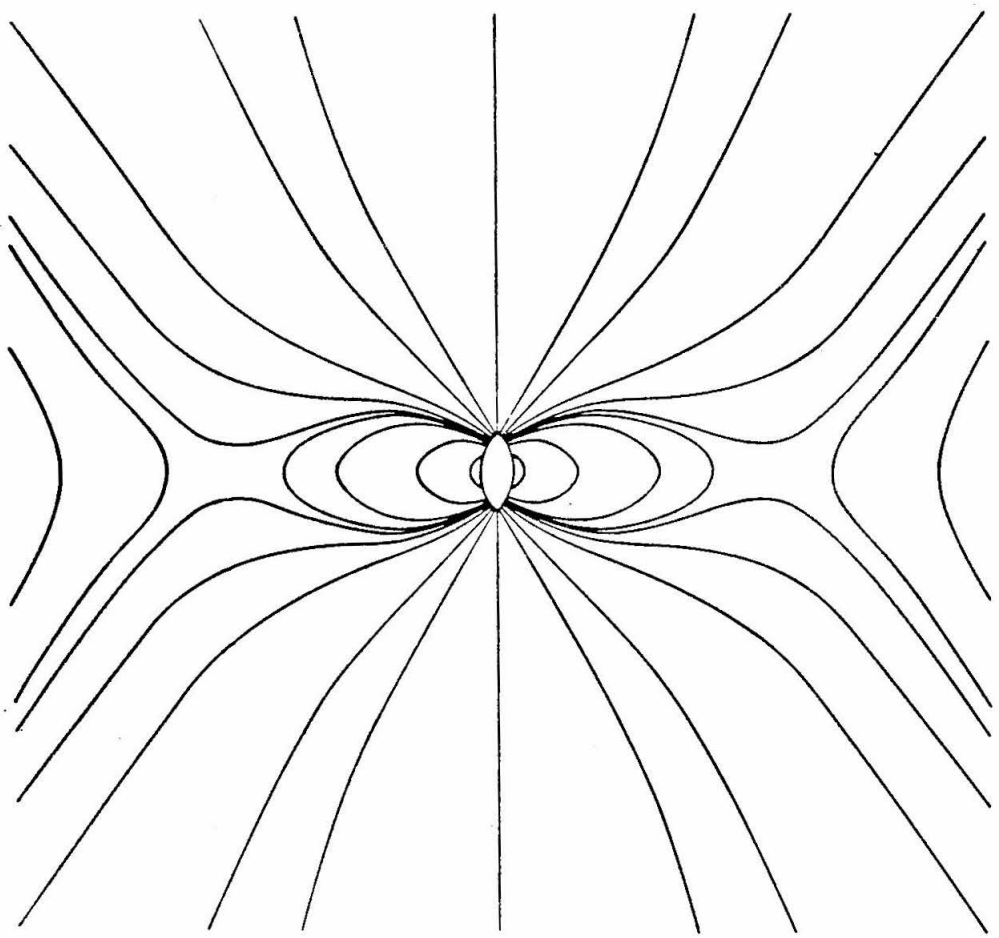

Figure 7. The streamlines ψ/c^2U in the laboratory frame for a prolate spheroid having eccentricity 0.9 for the case $V_n/U = 0$, $V_s/U = 1.17$.

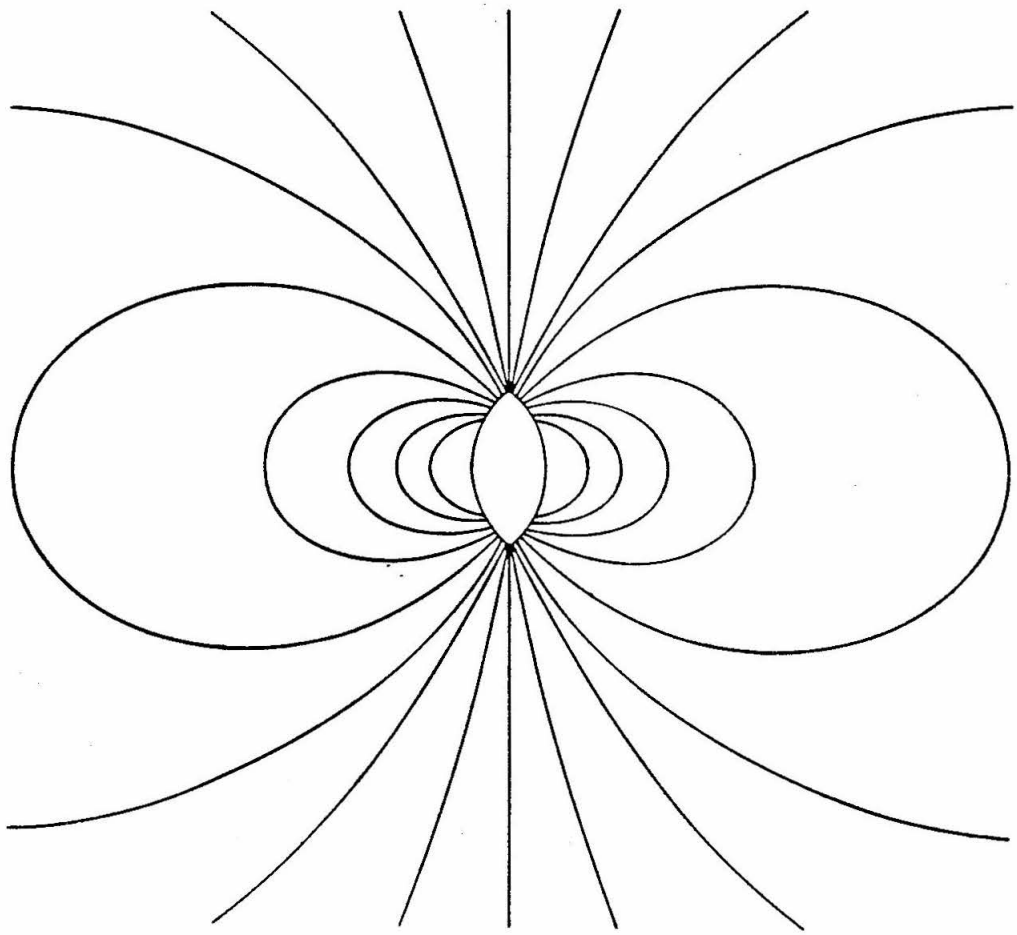

Figure 8. The streamlines $\psi/c^2\beta$ in the laboratory frame for a self-propelling prolate spheroidal body.

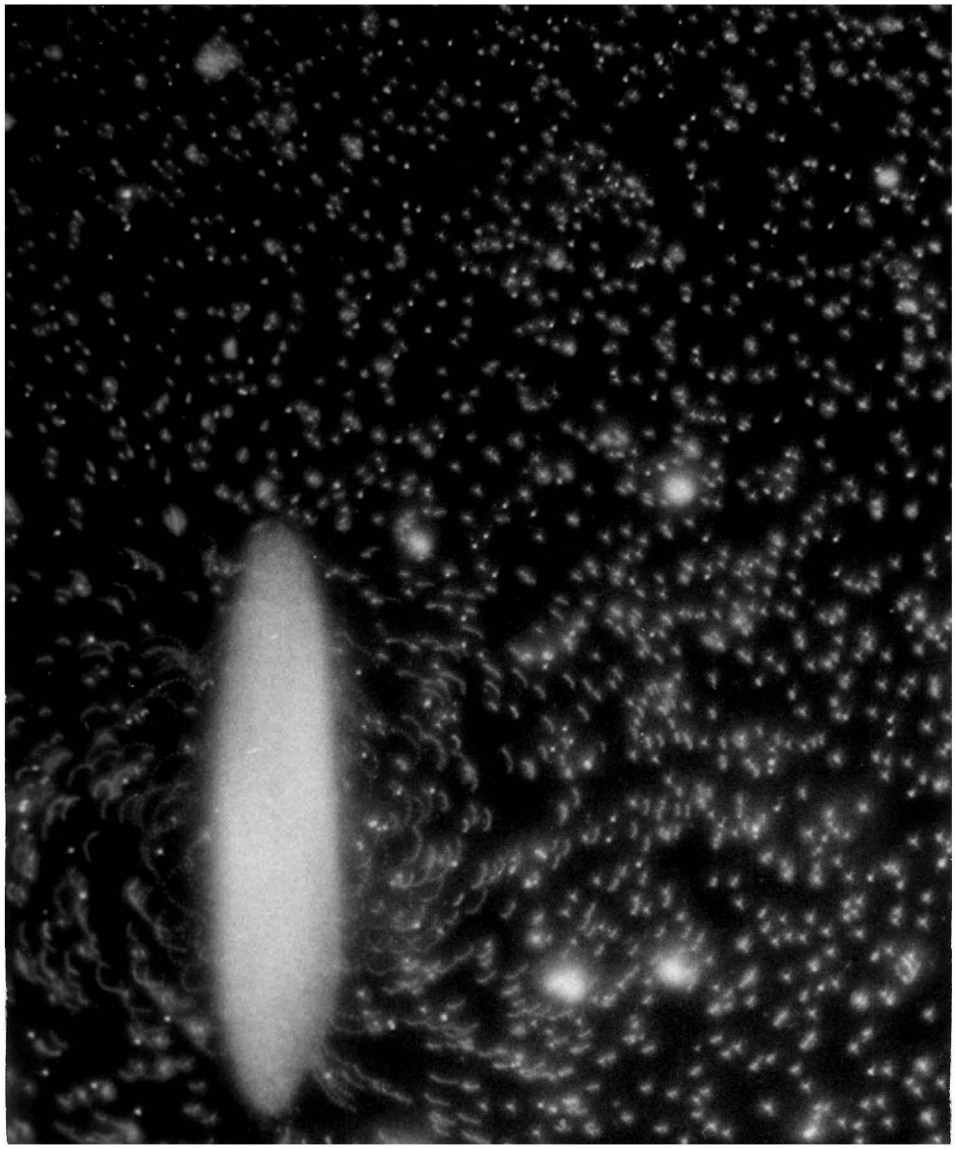

Figure 9. Streak photograph of a freely swimming Paramecium caudatum.

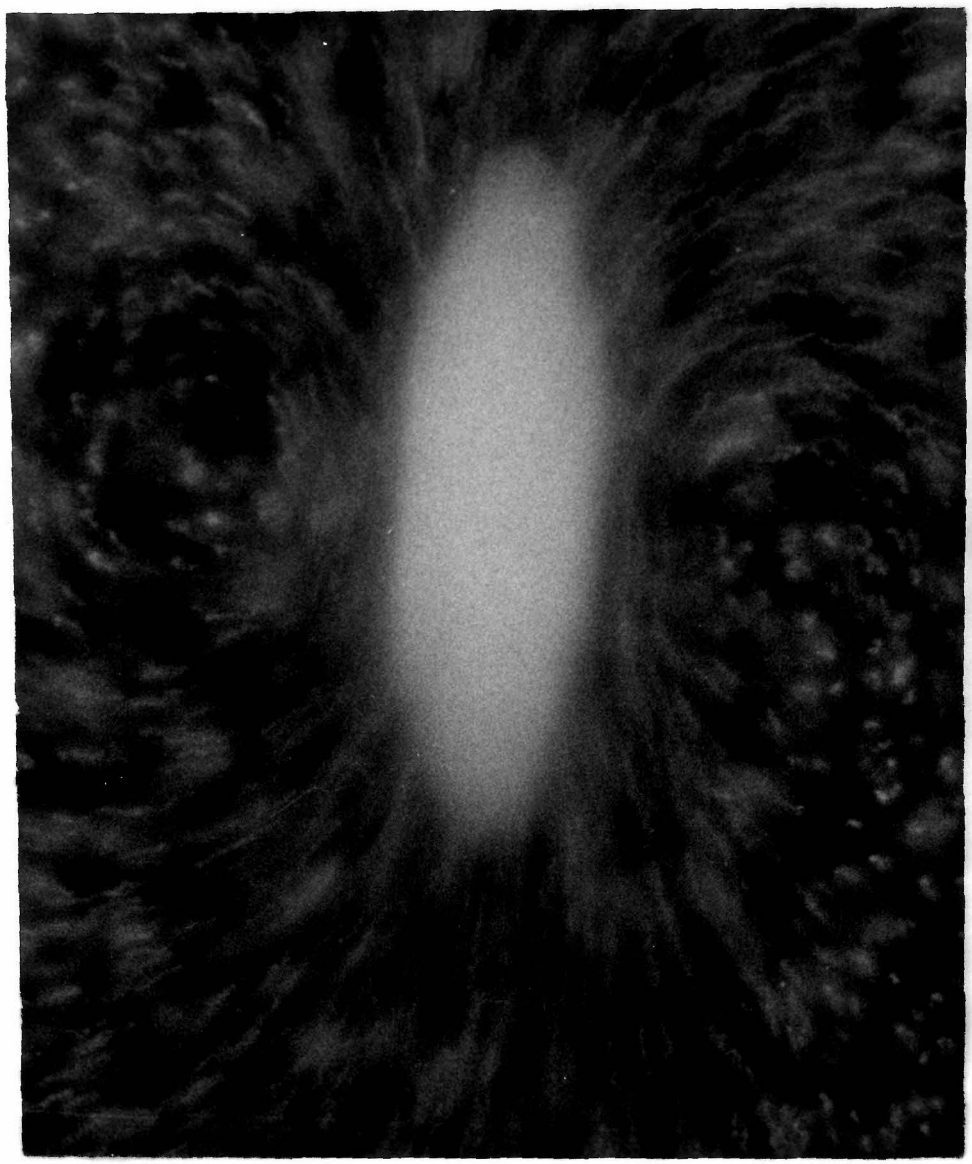

Figure 10. Streak photographs of a dead Paramecium caudatum falling under the influence of gravity.